POLITECNICO DI MILANO

School of Industrial and Information Engineering
Master of Science in Mechanical Engineering

Dynamic Analysis and Design of a 6-dof Parallel Mechanism Based on 6-PUS Kinematic Chains

Under Supervision of

Dott. Ing. Hermes Giberti

M.Sc Thesis of

Mohammad Izadi

Matr. 779460

Academic Year 2012 - 2013

Abstract

In this thesis the analysis of a 6-dof robotic platform based on the parallel architecture of Hexaglide has been done. The objective of the mechanism under study is to be applied as a test rig to perform unsteady aerodynamic experiments inside the wind tunnel. The 6-dof platform is intended to function as emulator in the loop of the sea to simulate the real working condition of the offshore structures.

Hexaglide, is a 6-dof fully parallel manipulator with 6 independent kinematic chain of PRRS type. Each kinematic chain is consist of an actuated prismatic joint on the base which is followed by a universal joint connecting the constant length link to the sliding body, which itself is followed by a spherical joint on the connection between link and platform.

Despite the advantageous performance features of parallel robots in terms of precise accuracy, fast operation speed, and high load capacities with respect to classic serial manipulators their application have been limited in practice. This is mainly due to their complexity of kinematics and dynamics problem which lead to difficulty of establishing a control law based on the dynamic model.

The analytical method to solve the inverse kinematic problem of the Hexaglide architecture has been represented. Also a formalism based on Newton-Euler equations of motion for the dynamic model is included. Then the multibody dynamics software Adams has been applied to perform the simulations. Based on the results of the dynamic simulation the design features of the robot have been discussed.

Acknowledgment

I would like to express my deepest gratitude to my supervisor, Prof. Hermes Giberti, for his excellent guidance, patience, and providing me with an excellent atmosphere for doing my research. Special thanks to Eng. Daniele Catelani, for guiding my research and helping me to develop my knowledge in the field of multibody dynamic analysis through the numerous beneficial discussion, and also by providing me every needed resources which helped me to carry my research. I would like to thank Eng. Davide Ferrari, and Eng. Navid Negahbani, who as a friend were always willing to help and give their best suggestions.

Contents

Chapter 1 Introduction 1

1.1 Different mechanism architectures 1

1.1.1 Serial architecture 1

1.1.2 Parallel architecture 3

1.1.3 Hybrid architectures 4

1.2 Performance features 5

1.2.1 Load/Mass ratio 5

1.2.2 Operation speed 6

1.2.3 Positioning accuracy 6

1.2.4 Rigidity 7

1.2.5 Workspace 9

1.2.6 Kinematic Analysis 9

1.3 6 dof parallel mechanisms 10

1.3.1 6UPS manipulators 12

1.3.2 6PUS manipulators 12

1.3.3 6RUS manipulators 14

1.4 Organization of the thesis 15

Chapter 2 Inverse kinematics 18

2.1 Description of the mechanism 20

2.2 Analytic solution of the Inverse kinematic problem 22

2.2.1 Inverse kinematic problem for position 22

2.2.2 Inverse kinematic problem for velocity 25

2.2.3 Inverse kinematic problem for acceleration 28

2.3 Simulation and motion analysis 28

Chapter 3 Dynamics 31

3.1 Description of the dynamic model 32
3.2 Analytic solution of dynamic problem 34
3.3 Simulation 41
3.3.1 Create geometry 41
3.3.2 Simulation with TCP imposed motion 43
3.3.3 Simulation with prismatic joints imposed motion 43
3.4 Discussion of the links mass and inertia 44
Chapter 4 Design 48
4.1 Work space definition 48
4.2 Description of the motion laws of TCP 49
4.3 Description of the method of automating simulations 51
4.4 Design Features 55
4.4.1 Alternative passive joints 55
4.4.2 Actuators design 56
4.5 Results 60
Conclusion 72
Appendix A 74
Appendix B 76
Appendix C 80
References 87

List of Figures

Figure 1-1 4-dof serial robot SCARA 2
Figure 1-2 the spherical parallel mechanism proposed in 1928 by J.E. Gwinnet [1] 3
Figure 1-3 an example of hybrid architecture 5
Figure 1-4 6UPS architecture flight simulator - Lufthansa 8
Figure 1-5 different kinematic chains configurations consist of prismatic, universal, and spherical joints [7] 11
Figure 1-6 The three main types of 6-DOF fully-parallel manipulators with identical kinematic chains designated as (a) 6-UPS, (b) 6-PUS, and (c) 6-RUS 12
Figure 1-7 Left: HexaM milling machine by Toyoda [12]; Right: HexaM architecture . 13
Figure 1-8 Left: Linapod architecture with vertical guide ways [13]; Right: Hexaglide robot ETH Zurich [14]. 14
Figure 1-9 Left: Hunt's 6RUS manipulator [15]; Right: Hexa robot [17] 15
Figure 2-1 kinematic model the i-th kinematic chain of the 6PUS manipulator 20
Figure 2-2 architectural families classified by symmetry type and height of rails 25
Figure 2-3 comparison between the inverse kinematic solution of the analytic algorithm and Adams FEA solver – generic motion law: 1 29
Figure 2-4 comparison between the inverse kinematic solution of the analytic algorithm and Adams FEA solver – generic motion law: 2 30
Figure 3-1 External and joint action forces applied on the robot 32
Figure 3-2 effect of mass and inertia on the magnitude force of the universal joint of the first kinematic chain 45
Figure 3-3 effect of mass and inertia on the magnitude force of the spherical joint of the first kinematic chain 45
Figure 3-4 Components of force of the universal joint of the first kinematic chain, projected to the local frame with z axis along the link 46
Figure 3-5 Magnitude force of the universal and spherical joint of the first kinematic chain 47
Figure 4-1 Description of the workspace of the robot 49
Figure 4-2 Macro command to execute the simulations of motion law 4) mov.α 52
Figure 4-3 geometry of the model imported inside Adams 53
Figure 4-4 Create request to store the linear actuating force of the prismatic joints 54
Figure 4-5 Spherical joints of INA and Hephaist Seiko (pictures courtesy of INA-Schaeffler KG and Hephaist Seiko) [7] 55
Figure 4-6 (a) The base universal joints and (b-d) three alternatives for the mobile platform spherical joints. 56

Figure 4-7 Comparison between different linear motion generators. The distant from the center indicate the convenience of the performance feature. [11] 57
Figure 4-8 Ball screw linear actuator DGE-SP Festo 58
Figure 4-9 Toothed Belt drive DGE-ZR Festo 59
Figure 4-10 Scheme of the model of the wind generator prototype test 62
Figure 4-11 Maximum actuating force of the kinematic chain 1, motion law: 4)mov.α 63
Figure 4-12 Maximum actuating force of the kinematic chain 2, motion law: 4)mov.α 63
Figure 4-13 maximum actuating force of the kinematic chain 3, motion law: 4)mov.α..... 64
Figure 4-14 maximum U-joint magnitude force of the kinematic chain 1, motion law: 4)mov.α 65
Figure 4-15 Left: Robot home position Right: Robot state correspond to maximum value of the linear actuating force of first kinematic chain 66
Figure 4-16 maximum slider reaction force FAi,z for the first kinematic chain, motion law: 4)mov.α 67
Figure 4-17 maximum slider reaction force FAi,z for the second kinematic chain, motion law: 4)mov.α 67
Figure 4-18 maximum slider reaction force FAi,z for the second kinematic chain, motion law: 4)mov.α 68
Figure 4-19 Left: Robot home position Right: Robot state correspond to maximum constraint reaction force FAi,z of first kinematic chain 68
Figure 4-20 maximum actuating force of all the kinematic chains, motion law: 3)mov.z . 69
Figure 4-21 maximum slider constraint reaction force along z axis of all the kinematic chains, motion law: 3)mov.z 69

List of Tables

Table 1-1 Characteristics of industrial manipulators Scara type [7] 7
Table 2-1 description of the parameters used in the kinematic problem 22
Table 2-2 Geometric parameters of the mechanism 28
Table 2-3 Motion trajectory definition of the platform 29
Table 3-1 Description of the parameters used in the dynamic problem 33
Table 3-2 Mass and inertia properties of the mechanism 42
Table 3-3 Motion law of the TCP for the dynamic simulation 44
Table 4-1 description of the motion laws applied to the TCP 50
Table 4-2 Mass and inertia properties of links 61
Table 4-3 Mass and inertia properties of platform 61
Table 4-4 Mass properties of sliders 61
Table 4-5 geometry and mass properties of the wind generator prototype 62
Table 4-6 maximum value of the loads on the sliders 70
Table C.1 maximum value of dynamic loads for the motion law: 4)mov.α 80
Table C.1 maximum value of dynamic loads for the motion law: 2)mov.y 82
Table C.3 maximum value of dynamic loads for the motion law: 3)mov.z 83

Chapter 1 Introduction

The concept of application of parallel architecture mechanisms has been proposed many years ago, as early as 1928 by J.E. Gwinnett [1] to be used as a platform for a movie theater (figure 1.2)[2].However, their practical applications have been limited due to the complexity of their analysis and control algorithm. With the development of the computational methods and powerful computers the parallel kinematic mechanisms have drawn attention during recent years in many different application fields. Their outstanding performance characteristics compared to classical serial robots in terms of fast and precise operations with high loads made them a convincing solution for applications such as flight simulators [3], industrial machines [4], and medical robotics [5] [6].

In this thesis a 6 degree of freedom parallel manipulator aimed to be used as the platform of the unsteady aerodynamic test rig in the wind tunnel has been analyzed. With respect to the growing interest in the field of renewable energies, it is convincing to develop new technologies to improve the energy conversion efficiency. In wind power technology, the advantage of offshore resources is that the wind is much stronger off the coasts. By applying the hardware in the loop simulation of the sea with the parallel manipulators it is possible to develop a test rig to realize the behavior of the offshore wind turbines through unsteady aerodynamic experiments inside the wind tunnel. Furthermore, it is possible to apply the platform for similar applications such as sailboats maneuvers tests.

In the next section the advantageous features of parallel manipulators with respect to serial manipulators for this application has been described.

1.1 Different mechanism architectures

1.1.1 Serial architecture

In serial architecture, the end-effector is linked to the base with a series of linkages and joints all in an open loop chain. Each rigid linkage is connected to the adjacent one by an active joint. In most cases, the joints applied in the serial manipulators are

usually of one dof, where allows the linkage to rotate around an axis respect to the adjacent one by a revolute joint, or one linear translational degree of freedom between two adjacent rigid body along the prismatic joint axis. Moreover, all the joints in the serial mechanisms are active kinematic pairs and all should be controlled during the function of the robot. With the succession of the actuated joints in the serial manipulators, it is possible to control the number of dof of the end-effector equal to the number of actuated joints.

A well known example of this type of robots architecture is the SCARA-Selective Compliance Assembly Robot Arm, figure 1.1. it is consist of two coplanar rigid links connected to each other and the base in succession by two revolute joints, and the end-effector connected to the second link by a prismatic joint which its axis is perpendicular to the plane of the two preceding link. In total this assembly gives the end-effector 3 d.o.f. In some applications, the end-effector also posses a rotational degree of reedom about the axis of the prismatic joint.

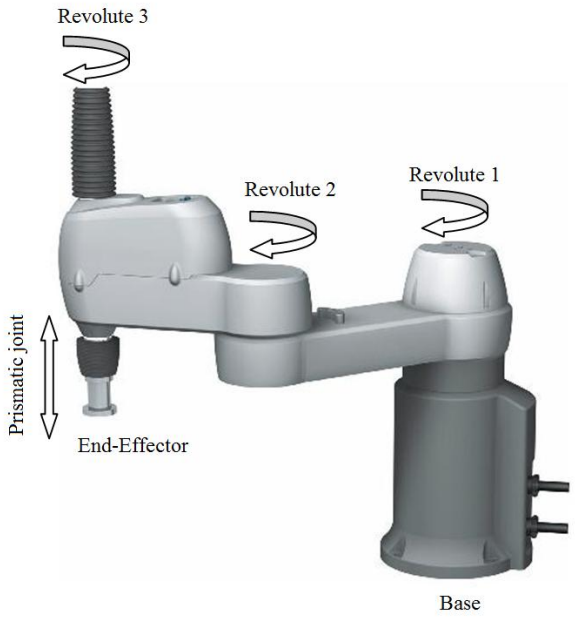

Figure 1-1 4-dof serial robot SCARA

1.1.2 Parallel architecture

In parallel architecture, the linkages that connect the base to the end-effector are not all in successive manner, but instead the end-effector is linked to the base by several kinematic chains working in parallel and independently from each other. The motion of the platform is applied by more than one kinematic chain acting on the end-effector simultaneously. The most significant difference between serial and parallel manipulators is that the parallel one includes closed loop kinematic chains in its architecture. A closed-loop kinematic chain is one in which the links and joints are arranged such that at least one closed loop exists [8](see appendix A).

Possibly the first parallel mechanism was designed by James E. Gwinnett[1] who applied for a patent in 1928 (figure 1.2) [2]. This device was based on a spherical parallel mechanism to be used as a platform for a movie theater.

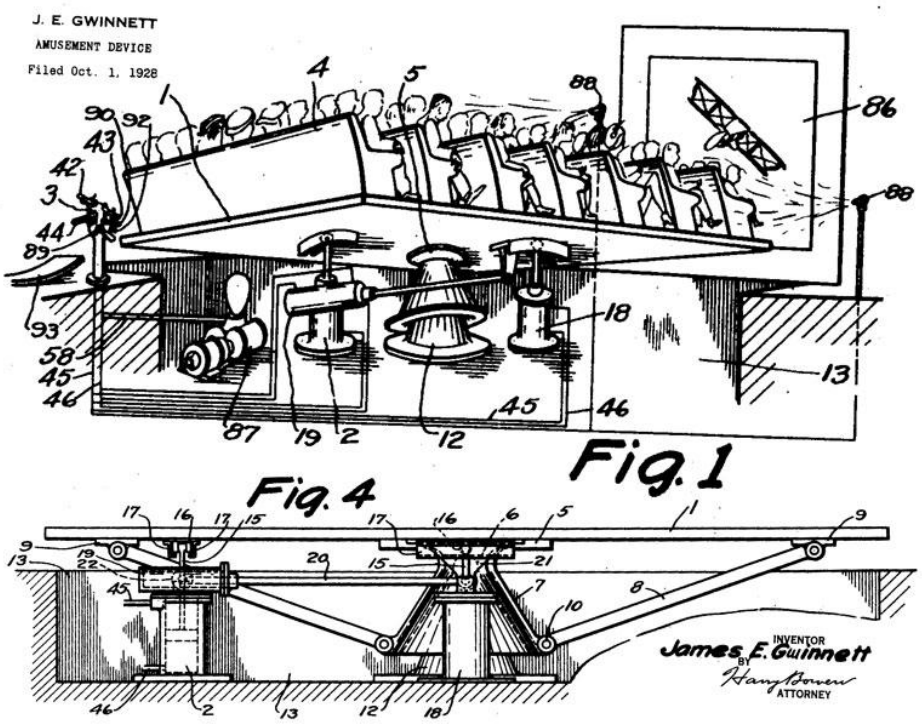

Figure 1-2 the spherical parallel mechanism proposed in 1928 by J.E. Gwinnet [1]

Another architectural difference between serial and parallel manipulators is that, parallel architecture includes both actuated and non actuated joints. The passive joints coordinates is defined by the coordinates of the active joints and the end-effector in the closed loop chain.

The definition of the parallel robots that mentioned could be stated as General Parallel Manipulators based on Merlet [7]. This definition is too general and includes many different types of architectures. A more specific type of general parallel manipulators is defined as the fully parallel manipulators: Parallel robots for which the number of chains is strictly equal to the number of dof of the end-effector, and each kinematic chain include only one actuating joint [8].

Using the general formula of mobility of Grübler for the fully parallel manipulator with m dof in 3D space we can write:

$$m = 6(n - j - 1) + \sum_{i=1}^{j} f_i \tag{1.1}$$

Where n is the total number of rigid bodies,j is the number of joints, and f_i is the number of dof of each joint. However, in parallel robots one should consider also the geometrical relations between the linkages in each closed loop kinematic chain for a more precise mobility analysis (See appendix A).

1.1.3 Hybrid architecture

Another architecture solution for robotic manipulators is hybrid design in which a combination of both parallel and serial architecture is applied. This kind of architecture is able to make a compromise between both advantages and disadvantages of parallel and serial robots. In figure 1.3 an example of hybrid solution discussed by K. Tanev[9] is given. This hybrid robot manipulator consists of two serially connected parallel mechanisms. Each mechanism has three degrees of freedom, so that the overall degrees of freedom of the robot are six.

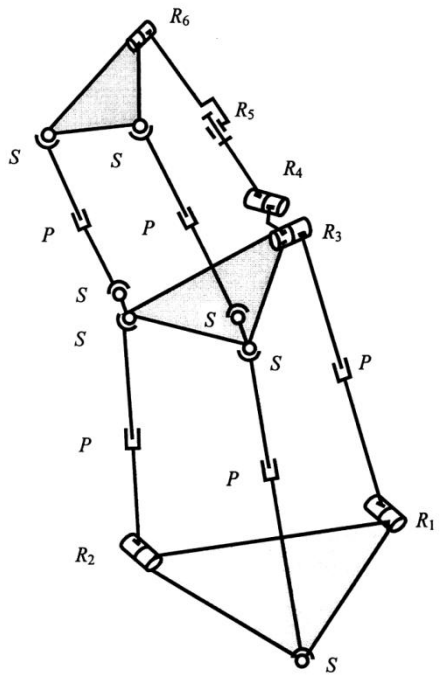

Figure 1-3 an example of hybrid architecture

1.2 Performance features

Comparing the serial and parallel manipulators in terms of performance, there are some applications that the parallel robots are advantageous and some other that the serial one. Here some aspects of robots with both architecture are explained and the well suited applications of each architecture based on their performance features are described.

1.2.1 Load/Mass ratio

The first advantage of parallel respect to serial manipulators is their capability of working with heavy loads. This leads to some applications of parallel robots where high loads are required. For serial manipulators the value of load/mass ratio could never be more than 0.25 in practice. This is mainly due to the fact that the linkages are mounted on each other successively, and so each actuator must also support the

weight of all successor Linkages, which demands also powerful motors. On the other hand, with parallel manipulators the weight of each closed loop kinematic chain doesn't affect on the other chains linkages and each kinematic chain work independently from other and support only a fraction of the end-effector load. For example considering a 6 dof fully parallel manipulator consist of 6 kinematic chain, where each kinematic chain include only one actuating joint, each actuator will support approximately only 1/6 of the load when the manipulator is performing in its central position with a rather symmetric condition.

Moreover, the weight of actuators mounting on the connection of linkages in serial robots has a significant effect in increasing the overall mass of the architecture and wasting the power of motors to support the actuators weight. In parallel robots, there is possibility of designing the architecture so that mounting all the actuators on the base, and decreasing the overall mass of the mechanism.

1.2.2 Operation speed

The successive linkages architecture of the serial manipulators becomes more disadvantageous when dealing with the dynamics of the robot. The large number of moving parts connected to each other in the serial chain leads to high inertia effects. This high inertia of serial manipulators cause problem when dealing with fast operations with high velocity and accelerations, such as fast pick and place tasks, or flight simulators. Furthermore, the fact that in some application it is possible to mount the actuators in the base, allows to use lighter limbs also, consequently the overall moving mass of the robot and inertia effects is reduced, and higher speed movements can be performed.

1.2.3 Positioning accuracy

There are different factors that affect the positioning accuracy of a robot such as the accuracy of the sensors that are used to measure the joints coordinate, or the deflection of the linkages, or the tolerances and quality of the geometrical features of the bodies. In general, the accuracy of the parallel robots is better than serial manipulators. This is due to the fact that, in the serial architecture of the kinematic chain each link must support the weight of the part of the chain following it in addition to the end-effector loads, which cause higher deflection and decrease the positioning accuracy. Also, since in parallel robots the loads are mostly in compression or tension form the deflection error is less than serial architecture

where the mechanism is highly subjected to torques. Moreover, compare to the parallel robots, in serial manipulators, the positioning error is build up due to the succession of the linkages, where in parallel it is possible to average out the error. The low accuracy of the serial robots leads to expensive and extremely accurate components.

In table 1.1 the poor performance features of some commercial serial robots in terms of load/mass ratio and accuracy can be seen.

Robot	dof	Mass [kg]	Load [kg]	Repeatability[mm]	Load/Mass
Adept I800	4	34	5.5	$\pm$ 0.02	0.1617
Adept 1XL	4	265	12	$\pm$ 0.025	0.0452
Adept 3XL	4	266	25	$\pm$ 0.038	0.0939
Epson E2C251	4	14	3	$\pm$ 0.01	0.21442
Epson E2S45x	4	20	5	$\pm$ 0.015	0.25
Epson E2H853	4	37	2	$\pm$ 0.025	0.054
Seiko EC250	4	14	3	$\pm$ 0.01	0.21438
Seiko EH850	4	43	10	$\pm$ 0.025	0.2325
Toshiba SR-504HSP	4	38	2	$\pm$ 0.02	0.0526

Table 1-1 Characteristics of industrial manipulators Scara type [7]

In general the repeatability of the robot is more precise than its absolute accuracy, but in practice the absolute accuracy is more important. However, still the repeatability of the serial robots shows a poor value.

1.2.4 Rigidity

One of the most important factors in term of performance of the robotic manipulators is the rigidity of the mechanism. Rigidity can directly affect the accuracy of the manipulators. Generally, the parallel architecture shows a better rigidity than the serial one. The open loop structure of serial robots is more subjected to bending loads and torques compared to the closed loop kinematic chain of parallel manipulators, where the forces are applied mostly in compression or traction along the direction of the links, and in general the axial stiffness of the linkages is higher than the bending one.

In serial architectures, the proper rigidity can be achieved by using more expensive high quality joints, and more massive linkages, which it leads to increase the amount of energy necessary to drive the motors also. On the other hand, in parallel manipulators it is possible to achieve a good rigidity with small mass, and consequently lower energy is necessary and also faster movements with precise accuracy can be achieved.

Figure 1-4 6UPS architecture flight simulator - Lufthansa

The high load/mass ratio and good rigidity of the parallel robots together with the ability of performing fast movements with high speed made them a convincing solution for some unique applications such as flight simulators figure 1.4.

On the other hand there are some negative aspects with parallel architecture respect to the serial one.

1.2.5 Workspace

The workspace can be defined as the region which can be reached by a reference point – TCP: tool center point – located on the mobile platform of the manipulator. The workspace has the same dimension as the number of degree of freedom of the manipulator. More particularly, the constant orientation workspace is defined as the position region which can be reached by the reference point of the manipulator when mobile platform has a specific prescribed constant orientation. Therefore, the constant orientation workspace has the same dimension as the number of translational degree of freedom of the manipulator.

The main disadvantage of parallel robots is their relatively low workspace. Due to existence of closed loop kinematic chains in parallel, the interference between the linkages is more likely than serial architectures, which leads to a limitation of designing a parallel architecture with ample workspace.

Also more singular configurations exist in the closed loop chains. The singularity is defined as the configurations of the robot that the joints velocity can not be projected in any end-effector space directions, consequently the joint actions must be infinitely larger to act on the end-effector.

The determination of the singular configuration for parallel robots is usually more complex, and so in general the works space is limited to small regions that it can be evaluated that no singular configurations exist.

1.2.6 Kinematic Analysis

Serial and parallel manipulators show contrary behavior in terms of kinematic analysis. Usually the solution of the direct kinematic problem for serial manipulators is obtained quite simply. The direct kinematic problem is defined as realizing the motion of the end-effector for a given set of joints coordinate motion law. The inverse kinematic problem is to define the joint coordinates corresponding to the given end-effector configuration. On the other hand, the inverse kinematic problem demands more complicated procedure, and in general a unique solution of the joints coordinate for a given end-effector coordinate does not exist.

This is due to the fact that we can not often write the equations in closed form, and furthermore we must solve sets of nonlinear equations with many unknowns and with multiple solutions. For example, we can obtain the same end-effector motion with different actuators motion law.

For parallel robots the situation is exactly reversed. The direct kinematic problem of the parallel robots is more complex than the inverse problem. The direct kinematic problem leads to multiple solutions, and the exact solution of the direct kinematic problem for parallel robots is only achievable if we know some information a priori about the current pose of the end-effector. Further, the inverse kinematic problem is rather simple.

In basic control algorithms, with only the inverse kinematic application, the multiple solution of the serial robots leads to some problems. However, in some applications, it is more likely to apply both inverse and direct kinematic in the control algorithm for a more proper performance.

Some other drawbacks of the parallel robots respect to serial manipulators can be mentioned as low dexterity, high anisotropy, and complexity of the dynamic analysis. It can be concluded that the most suited implementation of the parallel robots is in applications, where fast movements with precise accuracy are need in a limited work space.

1.3 6 dof parallel mechanisms

In this section different configurations of parallel manipulators with 6 degree of freedom are represented.

First a brief description of the different possibilities of synthesis of kinematic chains to generate motion are provided from Merlet [7]. In figure 1.5 is represented four different kinematic chains constituted by different synthesis of revolute, universal and spherical joints: RRPS, RPRS, PRRS, and RRRS, where RR stands for universal joint, and R and S are revolute and spherical joints respectively. In fully parallel manipulators, for each kinematic chain exist only one actuated joint, and the others are passive joints.

The RRPS kinematic chain which can be also stated as UPS chain, consist of an universal joint connected to the base, followed by a prismatic joint, and a spherical joint which is connected to the platform. Analogously, the RPRS kinematic chain is constituted by successively, a revolute joint followed by a prismatic joint on its axis, followed by another revolute joint and finally a spherical joint connected to the platform. The PRRS is consist of a prismatic, an universal, and a spherical joint successively, and in the same manner the last type RRRS is made of a revolute joint, followed by an universal and spherical joint respectively.

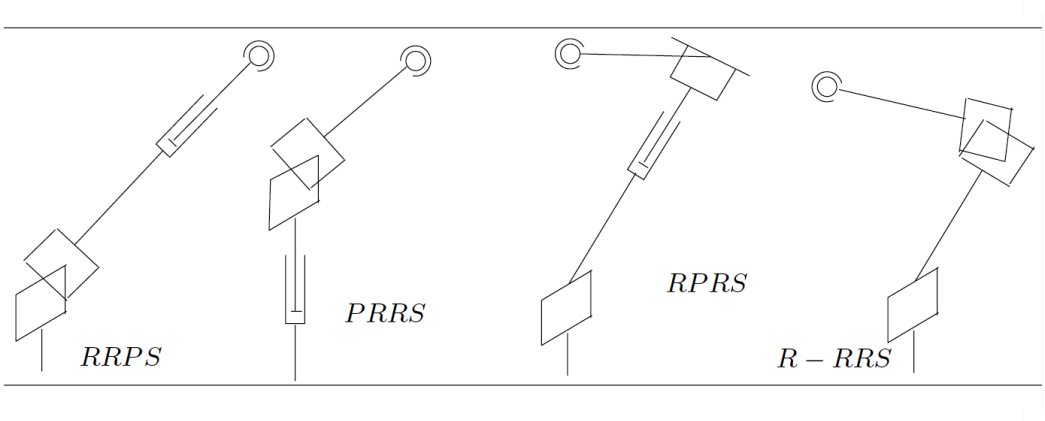

Figure 1-5 different kinematic chains configurations consist of prismatic, universal, and spherical joints [7]

A 6 dof fully parallel manipulator could be constituted by 6 kinematic chains of each of the types RRPS, RPRS, PRRS, and RRRS working in parallel, connecting the base to the platform. The motion is controlled in each kinematic chain by one actuated joint. We remind that the actuated joint could be any of the joints in the chain, but it is better to choose the joints on the base as the actuated one, and therefore decrease the moving mass and consequently the inertia forces of the mechanism and increase the performance of the robot in terms of high speed and accurate operations. Even though, all the parallel architectures formed by these different kinematic chains are equivalent in terms of mobility, but in terms of performance factors such as rigidity, and operation speed and also kinematic and dynamic analysis there is significant difference among them. In figure 1.6 three main types of the 6-dof fully parallel architectures with the mentioned kinematic chains are represented.

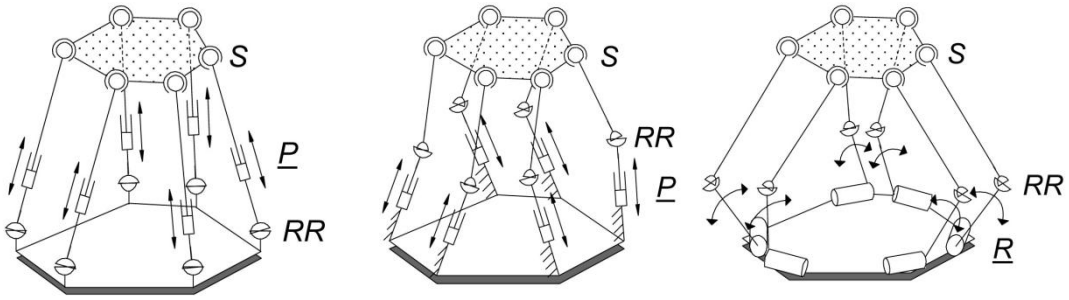

(a) (b) (c)

Figure 1-6 The three main types of 6-DOF fully-parallel manipulators with identical kinematic chains designated as (a) 6-UPS, (b) 6-PUS, and (c) 6-RUS.

1.3.1 6UPS manipulators

This is the most prominent architecture type of parallel robots. The first parallel robot with 6UPS architecture, where the underline stands for the actuated joints which is the prismatic one, was designed by Gough [26]. This type of manipulators are also well known as hexapod which are consist of 6 RRPS kinematic chains where the variation of the length of the links is given through prismatic joints and generate the motion of the manipulator. In most hexapods architectures the actuators are mounted on the link and so they are part of the moving components of the robot which leads to higher inertia loads. However, some other designs of hexapods exist where the linear actuators of screw type are mounted on the base and increase the length of the legs McCallion [27] and Shelef [18].

1.3.2 6PUS manipulators

In 6PUS or 6PRRS manipulators , each kinematic chain consist of a slider which is mounted on the base, followed by a universal joint that connects the slider to the link, and followed by a spherical joint that connect the link to the platform. The most significant difference compared to the 6UPS manipulators is that in the 6PUS manipulators the length of the links are constant, and instead the motion is generated by the linear actuators mounted on the base. This configuration has a better performance in terms of fast movements and accuracy respect to the

hexapods, mostly due to the fact that the actuators are not mounted on the moving parts of the structure. Furthermore, the probability of the interface between linkages in 6PUS manipulators is decreased due to the fact that the legs are of constant length and are only thin rods, where in 6UPS manipulators the assembly of actuators and variable length links needs more space, consequently this leads to a better achievable workspace for 6PUS structure. However, the kinematic and dynamic analysis of this type of manipulators is more complex than the 6UPS manipulators.

Different configuration of 6PUS manipulators exist with different direction of the motion of the prismatic joints. For instance, the *HexaM* milling machine by Toyoda (figure 1.7) [12] is constituted by inclined rails, or *Linapod* (figure 1.8.L)[13] with only 3 vertical guide ways. Many other configurations of the 6PUS architectures exist, see literature [7].

Figure 1-7 Left: HexaM milling machine by Toyoda [12]; Right: HexaM architecture

The *Hexaglide* robot from Ecole Poly technique Federale of Zurich (figure1.8 R) [14], is the type of 6PUS manipulators that applies horizontal rails to guide the motion of the sliders. In this configuration there are only three rails which are in the same plane. The main advantage of Hexaglide is that its workspace along the

direction of the rails can be easily extended with a pure translational movement of the platform along the rails directions.

In this thesis a new optimized architecture based on Hexaglide, which is constituted by 6 rails that are not necessarily coplanar is been studied.

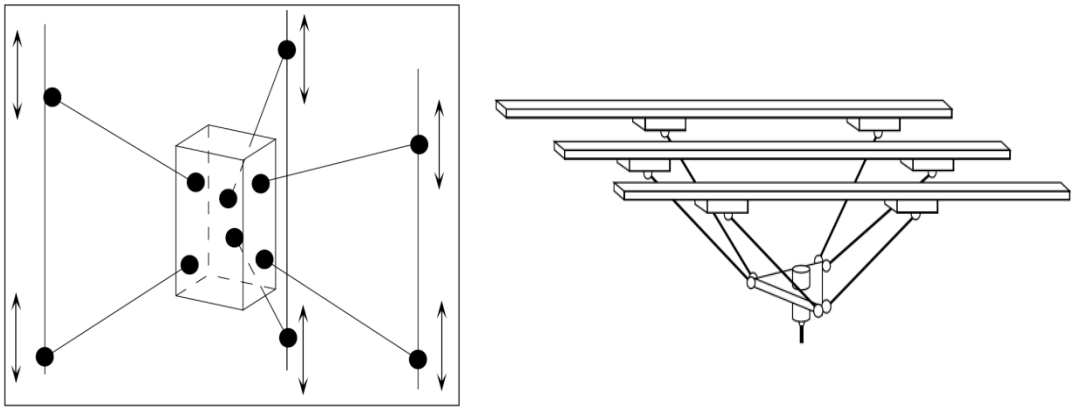

Figure 1-8 Left: Linapod architecture with vertical guide ways [13]; Right: Hexaglide robot ETH Zurich [14].

1.3.3 6RUS manipulators

Another architectural synthesis of the 6 dof parallel manipulators is the one with 6 independent kinematic chains of RRRS type. The first robot with this configuration was proposed by Hunt with actuating revolute joints (figure 1.9.L)[15]. Later, base on this architecture and the 3dof Delta constant orientation robot, Pierrot [16] and Uchiyama [17] proposed the 6 dof Hexa robot (figure 1.9.R). The difference between Hexa and Hunt's robot is in the location of the revolute joint on the base and the joint centers on the moving platform. Hexa robot is quite suitable for fast pick and place operations, since it shows a good performance in terms of speed and acceleration. However, the rigidity of this robot is reduced due to existence of corner angle in the middle of the arms at the location of the universal joints, and the universal joints are subjected to relatively high bending moments, therefore, the robot is not suitable for operation with high loads.

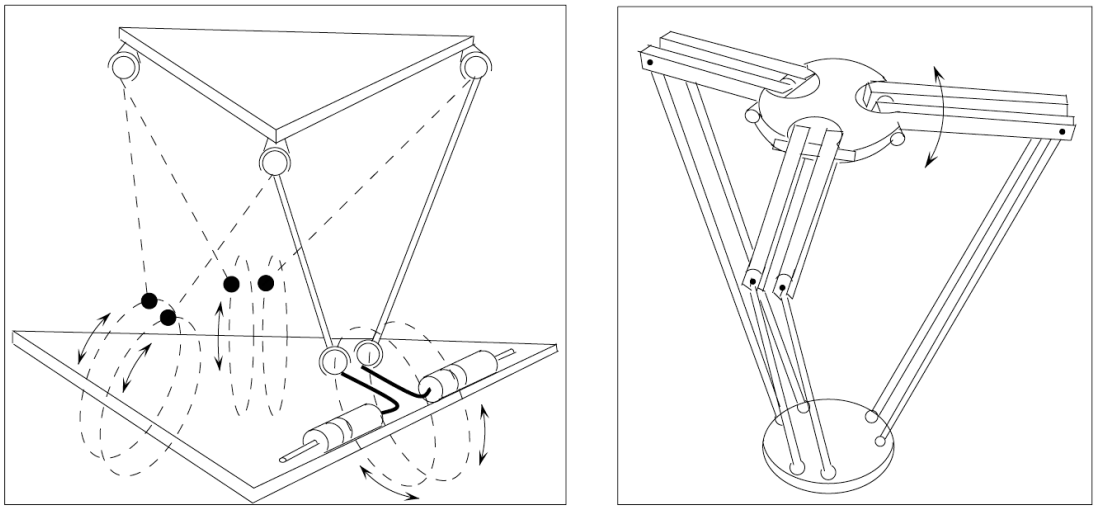

Figure 1-9 Left: Hunt's 6RUS manipulator [15]; Right: Hexa robot [17]

Obviously in Hexa architecture if the pair of links perform identical motion we will again have the constant orientation workspace for the platform with 3 dof which is similar to the Delta robot.

1.4 Organization of the thesis

This thesis is going to focus mainly on the dynamic behavior of a 6 degree of freedom parallel kinematic mechanism, based on the Hexaglide architecture. The objective is to realize the design features of the mechanism which are capable of generating the desired motion in the platform.

At the first step, in chapter 2 we have to determine the kinematics of the mechanism. We will point out the origins of the complexities of the direct kinematic of parallel manipulators, and the analytical method will be described to solve the inverse kinematic problem of the general 6PUS parallel manipulators and define the parameters that we need to apply in the upcoming chapter to solve the dynamic problem.

Based on the solution of the inverse kinematic, different architectural families of the 6PUS manipulators will be introduced. We also derive the inverse jacobian matrix necessary for the velocity analysis of the mechanism.

The geometrical description of the mechanism will be introduced under the consideration, which is obtained from the multi objective optimization method, and we apply the analytical method algorithm on this mechanism in a simulation phase and derive the time history solution of the displacement, velocity and acceleration of the actuating joints for a given motion law of the platform.

A model of the mechanism will be composed in Adams/view software, and perform another simulation using Adams finite element method to solve the inverse kinematic problem. Then, the results of the analytical method algorithm and the FEA of the Adams software will be compared.

In chapter 3, the direct and inverse dynamic problems of the manipulator are discussed. We will point out the application of the inverse dynamic in designing the mechanical components. Furthermore, the situations will be described in which the dynamics of the robot must be considered to compose the control algorithm. Then the problems are mentioned due to the complexity of the dynamics analysis of the parallel robots in the real time control. Also we represent some efforts that have been done to optimize the solution algorithm of the dynamic problem in terms of computation time.

An analytical method is represented to solve the inverse dynamic problem for the Hexaglide manipulators from Merlet [7]. Again we will apply Adams/view software finite element solver to perform the simulation on the mechanism under study, and describe the steps to solve the inverse dynamic problem.

Based on the solution of the inverse dynamic simulation for a generic motion law of the platform we will discuss some simplification considerations in the analytical method and evaluation of the forces in the rigid bodies of the mechanism.

Then a simulation will be performed again and the method will be described to simulate the robot in Adams/view in order to solve the dynamic problem of the

robot. We will point out some dynamic behaviors and design features of the robot according to the results of the simulation.

In the last section the method is illustrated to realize the dynamic behavior of the robot in its whole operation conditions by dividing the desired workspace into a grid of points. Many different simulations are performed in each point of the plane of the desired workspace with several motion laws of the platform. It will be described how to apply the macros in Adams/view to automate the work to deal with the huge number of simulations. Furthermore, a brief description of different alternatives for the joints configuration in 6PUS manipulators is given. Finally the results of the dynamic simulations necessary for designing the mechanical components are provided.

Chapter 2 Inverse kinematics

In this chapter the relations between the end-effector pose and the actuated joint coordinates necessary to perform the dynamic analysis are derived.

The study of the kinematic of robots divides in two main problems:

The direct kinematic problem is to realize the pose of the end-effector when the joints motions are defined.

The inverse kinematic problem however is to determine the relations in order to obtain the joints parameters for a specified pose of the end-effector.

In chapter 3 we are going to determine the joint actions for a specific imposed motion on the platform through inverse dynamic analysis. However, to solve the inverse dynamic the actuating joints coordinate and the relation between the actuating joints and passive joints coordinate must be defined. So the first step is to define the relations between the imposed motion of the platform and the joint coordinates. This is achieved by solving the inverse kinematic problem.

In case of serial robots the solution of the direct kinematic problem is rather simple. However, in case of inverse kinematics, we cannot often write equations in closed form, and furthermore we must solve sets of non-linear equations with many unknowns and with multiple solutions which leads to difficulty of the problem. In parallel architecture the situation is opposite. The direct kinematic problem leads to multiple solutions, and the exact solution of the direct kinematic problem for parallel robots is only achievable if we know some information a priori about the current pose of the end-effector.

Despite the forward kinematic problem, the analytic method to solve the inverse kinematic problem for parallel robots is simple. If the chains in the parallel robot do not share an actuated joint variable, the solution can be obtained in parallel for each chain. We will describe the analytical method to solve the inverse kinematic problem based on the approach described by Merlet[7].

We represent the reference frame with **O**, and the generalized coordinate of the moving platform with respect to the reference frame by **X**, and the chain joint coordinates with **Q**. Note that **Q** includes all the joints in a chain and not only the actuated joints. The solution of the inverse kinematic problem is to find **Q** when **X** is given.

For each of the chains linking the base to the moving platform we consider two extremities: point **A** which represent the end of the chain that is linked to the base and its coordinates are fixed and known with respect to the reference frame, And point **B** which is the other end of the chain, linked to the moving platform. The coordinates of **B** are known and usually fixed in the moving frame associated to the platform. Once the position of a point in the rigid platform and its orientation are given we can construct the rotation matrix **R** between the moving frame of the platform and the reference frame and hence the coordinates of point **B** could be obtained in the reference frame. Therefore, the position of point **B** in the reference frame is a function of **X**.

Therefore, the determination of the vector **AB** can play a fundamental role in the inverse kinematic analysis. We can write:

$$\mathbf{AB} = \mathbf{AO} + \mathbf{OB} = \mathrm{H}_1(\mathbf{X}) \tag{2.1}$$

On the other hand we can determine vector **AB** as a function of the joint coordinates and platform coordinate:

$$\mathbf{AB} = \mathrm{H}_2(\mathbf{X}, \mathbf{Q}) \tag{2.2}$$

By relating the above equations we can determine the relation between the platform coordinate and the joint coordinate:

$$\mathrm{H}_1(\mathbf{X}) = \mathrm{H}_2(\mathbf{X}, \mathbf{Q}) \tag{2.3}$$

In most parallel robots the chains are simple and so the solution can be obtained simply. Since **Q** includes also passive joints, by this method the coordinates of the passive joints can also be determined and not only actuated joints. The advantage is

that we can check also the spherical joints and universal joints coordinate in order to avoid violation of the range of joints.

However, we can avoid over calculation to determine all the joints coordinate and only finding the actuated joints variable by calculating the norm of the vector **AB** as it will be explained later. We can check the working range of the joints by considering the orientation of the links. To do this we need to determine the axes of the universal and spherical joints a priori for the home position of the robot, and by taking into account the orientation of links which can be obtained only by the position of the platform and the actuated joints we can check the working range of the passive joints also.

2.1 Description of the mechanism

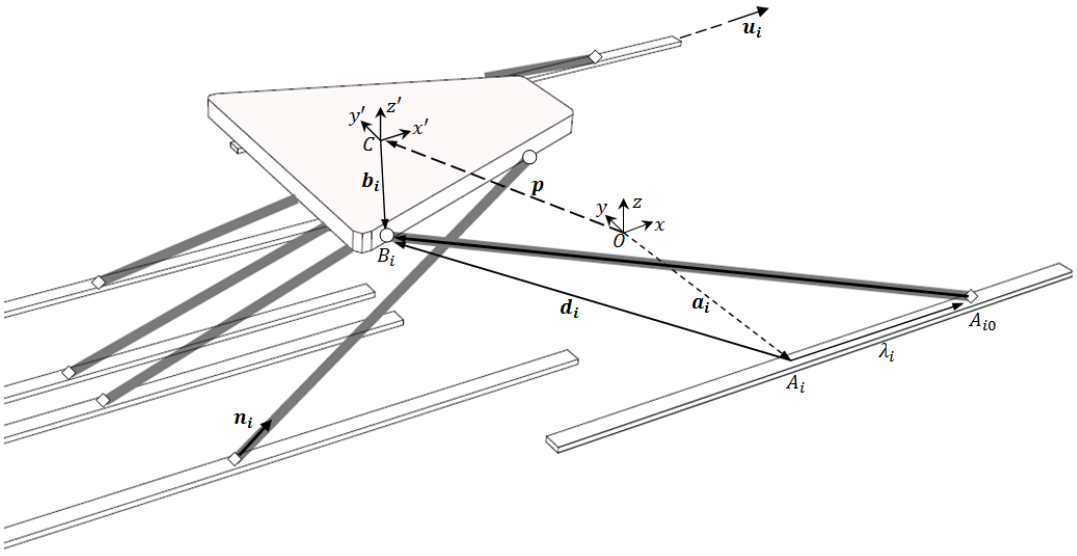

Figure 2-1 kinematic model the i-th kinematic chain of the 6PUS manipulator

Hexaglide is a 6-PUS fully parallel robot, consist of 6 legs of fixed length which are connected to 6 sliders on the rail through universal joints at one end and to the platform at the other end by spherical joints. The 6 degree of freedom motion is achieved through the 6 linear actuators mounted on the rails. The schematic of the mechanism is shown in figure 2.1.

We will derive the inverse kinematic relation based on the method introduced above. Referring to the figure 2.1 the following notation is introduced in the table 2.1 in order to describe the mechanism.

There are several ways to represent the pose of the platform. We use the most classical way which is the combination of the three coordinates describing the position of the TCP and the Euler angles to define the orientation of the moving frame of the platform with respect to the fixed reference frame. The orthogonal rotation matrix depends on the choice of the sequence of the rotations defining the Euler angles. (See appendix B)

symbol	Description
$O - xyz$	reference fixed frame attached to the base
$C - x'y'z'$	moving frame attached to the platform
C	tool center point of the platform (TCP)
A_i	starting point of the individual slider
A_{i0}	center of the individual slider/universal joint
B_i	center of the individual spherical joint
$\boldsymbol{b_i} \equiv CB_i$	position vector of point B_i with respect to the origin of moving frame, C and projected in the moving frame, $C - x'y'z'$
$\boldsymbol{b'_i} \equiv CB_{i,r}$	position vector of point B_i with respect to the origin of moving frame, C and projected in the fixed reference frame, $O - xyz$
$\boldsymbol{a_i} \equiv OA_i$	position vector of fixed point A_i in the fixed reference

	frame, $O-xyz$
$\boldsymbol{u_i} = [1 \quad 0 \quad 0]$	unit vector along the individual rail axis, projected on the fixed reference frame, $O-xyz$
$\boldsymbol{n_i} = [n_{i,x} \quad n_{i,y} \quad n_{i,z}]^T$	unit vector along the individual leg, projected on the fixed reference frame, $O-xyz$
λ_i	distant of the individual slider from the starting point
$\boldsymbol{\lambda} = [\lambda_1 \quad \lambda_2 \quad ... \quad \lambda_6]^T$	vector of the actuated joints coordinate
l_i	length of the individual leg
$\boldsymbol{d_i} \equiv A_iB_i = [d_{i,x} \quad d_{i,y} \quad d_{i,z}]$	vector linking the starting point of each chain on the base to the platform end point,B_i
$\boldsymbol{p} \equiv OC = [p_x \quad p_y \quad p_z]^T$	position of the TCP projected in the fixed frame,$O-xyz$
$\boldsymbol{\theta} = [\alpha \quad \beta \quad \gamma]^T$	vector of the orientation of the platform representing by Euler angles
$\boldsymbol{X} = [\boldsymbol{p} \quad \boldsymbol{\theta}]^T$	vector of pose of the platform
$\boldsymbol{\omega} = [\omega_x \quad \omega_y \quad \omega_z]^T$	vector of the angular velocity of the platform
$\dot{\boldsymbol{S}} = [\dot{\boldsymbol{p}} \quad \boldsymbol{\omega}]^T$	vector of the linear and angular velocity of the platform
$\boldsymbol{R}$	the 3 × 3 rotation matrix representing the orientation of moving frame,$C-x'y'z'$ with respect to fixed frame, $O-xyz$
$\boldsymbol{\Omega}$	the 3 × 3 skew symmetric matrix of angular velocity of the platform

Table 2-1 description of the parameters used in the kinematic problem

2.2 Analytic solution of the Inverse kinematic problem

2.2.1 Inverse kinematic problem for position

As mentioned before the inverse kinematic solution of parallel robots is rather simple. For the 6-PUS manipulator the actuated joint is the prismatic one on the rails. The inverse kinematic problem for position is to determine the sliders pose for a given coordinate of the platform. We denote C as the tool center point of the platform which its coordinate and orientation respect to the reference frame are defined by **X**. so the problem would be to define the length of A_iA_{i0} for a given **X**.

According to the figure 2.1 we can define the fundamental vector A_iB_i for each closed loop chain as:

$$\boldsymbol{d_i} = A_iB_i = OC + \boldsymbol{R}CB_{i,r} - OA_i = \boldsymbol{p} + \boldsymbol{Rb'_i} - \boldsymbol{a_i} = H_1(\boldsymbol{X}) \tag{2.4}$$

Where$CB_{i,r}$is the vector of position of point B_i projected in the moving frame, and its coordinate in the frame$C - x'y'z'$ is fixed and known. $\boldsymbol{R}$ is the rotation matrix of the moving frame with respect to the reference frame and is defined by the orientation of the platform which is known.

On the other hand we can define the vectors $A_iA_{i0}$and $A_{i0}B_i$ by the joint coordinates which are consist of the prismatic joint distance λ and the two rotation angels of the universal joint α_1, α_2 :

$$\boldsymbol{d_i} = A_iB_i = A_iA_{i0} + A_{i0}B_i = \lambda_i\boldsymbol{u_i} + l_i\boldsymbol{n_i} = H_2(\lambda, \alpha_1, \alpha_2) \tag{2.5}$$

By combining equations (2.4) and (2.5) we would have a system of 3 equations on 3 unknowns $(\lambda, \alpha_1, \alpha_2)$. However, we are only interested to determine the actuated joint coordinates which are λ_i. In order to do that we can simply evaluate the norm of vector $A_{i0}B_i$:

$$\boldsymbol{n_i}^T l_i l_i \boldsymbol{n_i} = l_i^2 = (\boldsymbol{d_i} - \lambda_i\boldsymbol{u_i})^T(\boldsymbol{d_i} - \lambda_i\boldsymbol{u_i}) = \boldsymbol{d_i}^T\boldsymbol{d_i} - 2\boldsymbol{d_i}^T\lambda_i - \boldsymbol{u_i}^T\lambda_i\lambda_i\boldsymbol{u_i} \tag{2.6}$$

Where all the rails are parallel to the x axis of the reference frame, $O-xyz$ and so the unit vectors $\boldsymbol{u_i} = [1 \quad 0 \quad 0]^T$So:

$$l_i^2 = d_i^2 - 2d_{i,x}\lambda_i + \lambda_i^2 \tag{2.7}$$

Finally the actuated joint parameters could be found by the equation below:

$$\lambda_i = d_{i,x} + h_i\sqrt{l_i^2 - d_{i,y}^2 - d_{i,z}^2} \qquad , \quad h_i = \pm 1 \tag{2.8}$$

Generally we would have two solutions for λ_i according to the quadratic equation (2.7). The choice of the coefficient h_i will lead to different architecture assembly of the mechanism.

One should pay attention to choose the solution which is compatible with the maximum range of the sliding actuators and avoid the contact between linkages. Furthermore, when choosing the value of h_i the constraints due to the allowed working range of the universal and spherical joints - passive joints - must be also considered. The coordinates of the passive joints of each kinematic chain, can be evaluated from the geometrical constraints of the closed loop kinematic chain, for a given pose of the end-effector and the solution of the inverse kinematic for actuating joints coordinates.

In order to ensure a symmetric global workspace with respect to the longitudinal vertical xz plane, the coefficients must be chosen so that the links and respective joints obey one of the following symmetry type With zero oriented platform at $y_{TCP} = 0$:

1- Symmetry with respect to the xz plane
2- Central symmetry with respect to z axis

Figure 2.2 shows the different families of the robot with different possible symmetry types:

- Family 1: three pair of links with symmetry type 1
- Family 2: two pair of links on opposite side with symmetry type 1 and one pair with symmetry type 2
- Family 3: two pair of links on the same side with symmetry type 1 and one pair with symmetry type 2
- Family 4: one pair with symmetry type 1 and two pair of links with symmetry type 2
- Family 5: three pair of links with symmetry type 2

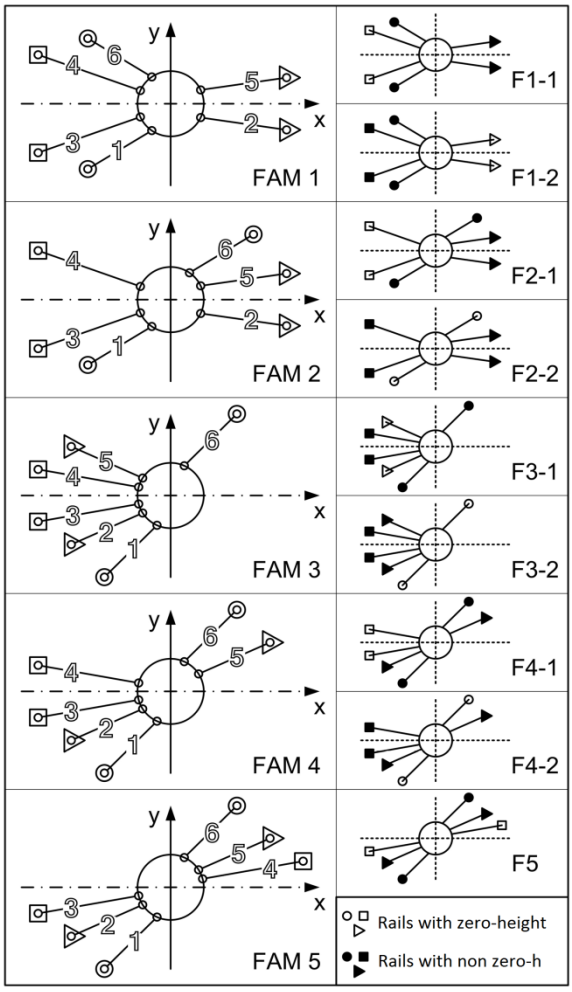

Figure 2-2 architectural families classified by symmetry type and height of rails

2.2.2 Inverse kinematic problem for velocity

To determine the relation between the velocity of the TCP and the actuated joints, we take the derivative with respect to time of the vector defining the length of the links from the equation (2.5):

$$\dot{l}_i \boldsymbol{n_i} = \dot{\boldsymbol{d}}_{\boldsymbol{i}} - \dot{\lambda}_i \boldsymbol{u_i} \tag{2.9.a}$$

Pre multiplying both sides by $\boldsymbol{n_i^T} l_i$:

$$\boldsymbol{n_i^T} l_i \dot{l}_i \boldsymbol{n_i} = \boldsymbol{n_i^T} l_i \left(\dot{\boldsymbol{d}}_{\boldsymbol{i}} - \dot{\lambda}_i \boldsymbol{u_i}\right) \tag{2.9.b}$$

The lengths of the links are constant so:

$$0 = \boldsymbol{n_i^T} \left(\dot{\boldsymbol{d}}_{\boldsymbol{i}} - \dot{\lambda}_i \boldsymbol{u_i}\right) \tag{2.9.c}$$

Replacing the expression $\boldsymbol{d_i}$from (2.4) and considering that the length of vectors $\boldsymbol{a_i}$, $\boldsymbol{b'_i}$ are constant:

$$0 = \boldsymbol{n_i^T} \left(\dot{\boldsymbol{p}} + \dot{\boldsymbol{R}} \boldsymbol{b'}_i - \dot{\lambda}_i \boldsymbol{u_i}\right) \tag{2.10.a}$$

Keeping in mind that $\boldsymbol{b}_i = \boldsymbol{R} \boldsymbol{b'}_i$:

$$0 = \boldsymbol{n_i^T} \left(\dot{\boldsymbol{p}} + \dot{\boldsymbol{R}} \boldsymbol{R^{-1}} \boldsymbol{b}_i - \dot{\lambda}_i \boldsymbol{u_i}\right) \tag{2.10.b}$$

In which $\dot{\boldsymbol{R}} \boldsymbol{R^{-1}} = \boldsymbol{\Omega}$ is the skew symmetric matrix of angular velocity of the platform (See appendix B)

From the property of the skew symmetric matrix, we can replace the expression $\boldsymbol{\Omega b}_i$ in the equation (2.10) with the cross product of the vector of angular velocity and the vector $\boldsymbol{b_i}$:

$$\boldsymbol{n_i^T} \dot{\boldsymbol{p}} + \boldsymbol{n_i^T} (\boldsymbol{\omega} \times \boldsymbol{b_i}) = \boldsymbol{n_i^T} \dot{\lambda}_i \boldsymbol{u_i} \tag{2.11}$$

In which $\boldsymbol{\omega} = \{\omega_x \omega_y \omega_z\}'$.

Keeping in mind that for the three vectors we have: $\boldsymbol{n_i} . (\boldsymbol{\omega} \times \boldsymbol{b_i}) = \boldsymbol{\omega}. (\boldsymbol{b_i} \times \boldsymbol{n_i}) = \boldsymbol{b_i}. (\boldsymbol{n_i} \times \boldsymbol{\omega})$ we can rewrite the equation (2.11):

$$\left[\boldsymbol{n_i^T} (\boldsymbol{b_i} \times \boldsymbol{n_i})^T\right] \begin{Bmatrix} \dot{\boldsymbol{p}} \\ \boldsymbol{\omega} \end{Bmatrix} = \boldsymbol{n_i^T} \dot{\lambda}_i \boldsymbol{u_i} \tag{2.12}$$

We define the vector, $\dot{\boldsymbol{S}} = \begin{Bmatrix} \dot{\boldsymbol{p}} \\ \boldsymbol{\omega} \end{Bmatrix}$. Notice that the vectors, $\dot{\boldsymbol{S}}$ and $\dot{\boldsymbol{X}}$ are not identical. The components of the angular velocity vector of the platform are related to the Euler angles defining the orientation of the platform, and their rate of changes. This relation depends on the choice of the sequence of the rotations of the Euler angles. (See appendix B)

By considering all the closed loop chain we can define the matrical relation between the platform velocity and the actuated joints velocity in the following matrical form:

$$\boldsymbol{J_p^{-1}}\dot{\boldsymbol{S}} = \boldsymbol{J_q}\dot{\boldsymbol{\lambda}} \tag{2.13}$$

Where:

$$\boldsymbol{J_q} = diag(\boldsymbol{n_{i,x}}) \tag{2.14}$$

$$\boldsymbol{J_p^{-1}} = \begin{bmatrix} \boldsymbol{n}_1^T & (\boldsymbol{b}_1 \times \boldsymbol{n}_1)^T \\ \vdots & \vdots \\ \boldsymbol{n}_6^T & (\boldsymbol{b}_6 \times \boldsymbol{n}_6)^T \end{bmatrix} \tag{2.15}$$

And the unit vectors along the legs can be defined by only the actuated joints parameter,λ_i and the position and orientation of the platform:

$$l_i\boldsymbol{n_i} = \boldsymbol{p} + \boldsymbol{b_i} - \boldsymbol{a_i} - \lambda_i\boldsymbol{u_i} \tag{2.16}$$

Therefore we can define the inverse Jacobian matrix as:

$$\boldsymbol{J}^{-1} = \boldsymbol{J_q}^{-1}\boldsymbol{J_p^{-1}} \tag{2.17}$$

So we have determined the relation between the velocity of the TCP and the actuate joints with the inverse Jacobian matrix:

$$\dot{\boldsymbol{\lambda}} = \boldsymbol{J}^{-1}\dot{\boldsymbol{S}} \tag{2.18}$$

2.2.3 Inverse kinematic problem for acceleration

In order to define the relation between the acceleration of TCP and the actuated joints we can take derivative of the velocity relation (2.18) defined by the inverse jacobian matrix in the previous section :

$$\ddot{\boldsymbol{\lambda}} = \boldsymbol{J}^{-1}\ddot{\boldsymbol{S}} + \dot{\boldsymbol{J}}^{-1}\dot{\boldsymbol{S}} \tag{2.19}$$

We remind here that in this relation we don't include the passive joints coordinate and the jacobian matrix defined is only relating the actuated joints velocity to the linear and angular velocity of the TCP.

The jacobian matrix defined in (2.17) is a function of the pose of both generalized coordinate of the platform and the actuated joints coordinate.

2.3 Simulation and motion analysis

We have solved the inverse kinematic problem for position, velocity, and acceleration of the mechanism by the algorithm defined in this chapter. In table2.2 the geometrical data of the mechanism under study are given. In order to perform the simulation two different motion laws on the TCP have been imposed, table 2.3. We assume that the initial position of the actuators is coincidence with point Ai.

	x [m]	y [m]	z [m]
A_1	-0.72394	-0.40574	0.07400
A_2	1.42874	-0.57501	0.19799
A_3	-0.91109	-0.13999	0.00000
A_4	-0.91109	0.13999	0.00000
A_5	1.42874	0.57501	0.19799
A_6	-0.72394	0.40574	0.07400
B_1	0.34400	-0.07283	0.56103
B_2	-0.03169	-0.34850	0.81105
B_3	0.19389	-0.12800	0.75803
B_4	0.19389	0.12800	0.75803
B_5	-0.03169	0.34850	0.81105
B_6	0.34400	0.07283	0.56103
C (TCP)	0.00000	0.00000	0.98000
O	0.00000	0.00000	0.00000

Table 2-2 Geometric parameters of the mechanism

	Motion law 1 : $f = 0.7\ [Hz]$	Motion law 2 : $f = 0.7\ [Hz]$
$x(t)\ [m]$	$0.5\sin(2\pi f.t)$	0
$y(t)\ [m]$	0	$0.3\sin(2\pi f.t)$
$z(t)\ [m]$	z_{TCP}	z_{TCP}
$\alpha(t)\ [deg]$	0	0
$\beta(t)\ [deg]$	0	0
$\gamma(t)\ [deg]$	0	15

Table 2-3 Motion trajectory definition of the platform

In another step, we have also applied the multi-body dynamic analysis software Adams finite element approach, in order to perform the simulation with same data. In the figure 2.3 and figure 2.4 the results of the simulation by both methods are given. The simulation is performed for 2 periods of the platform motion law, and the results are given below: it can be seen that the solution of both approaches are coincidence.

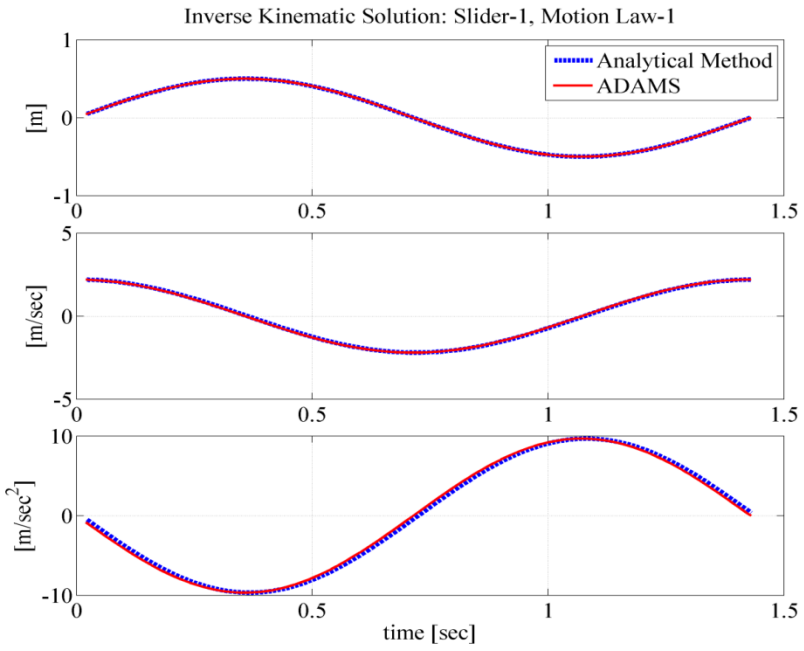

Figure 2-3 comparison between the inverse kinematic solution of the analytic algorithm and Adams FEA solver – generic motion law: 1

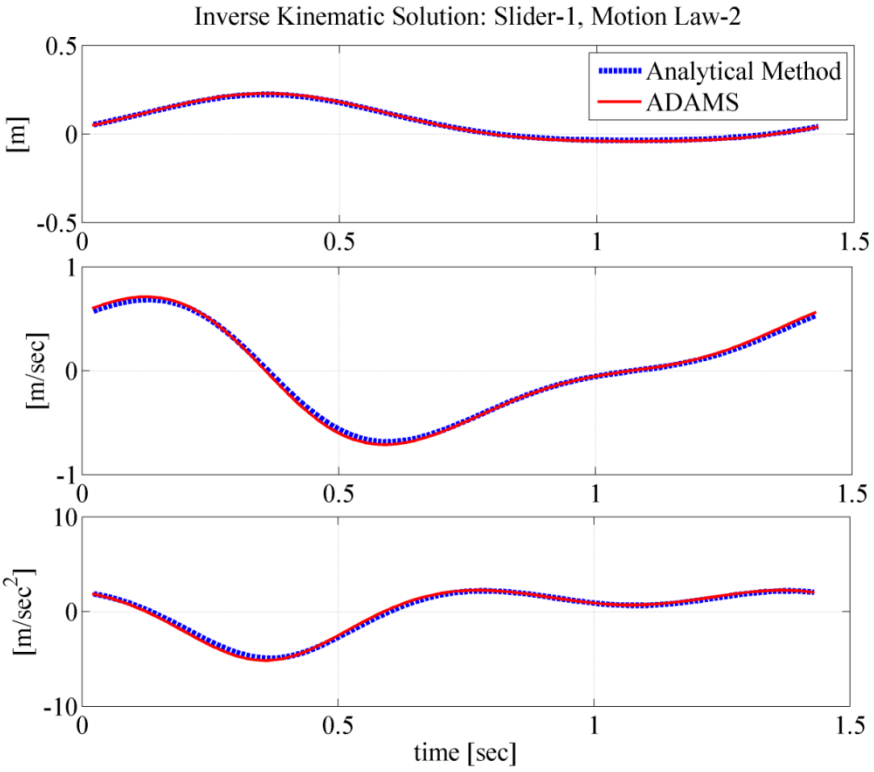

Figure 2-4 comparison between the inverse kinematic solution of the analytic algorithm and Adams FEA solver – generic motion law: 2

Chapter 3 Dynamics

This chapter is dedicated to the dynamics of the parallel robots, which defines the relations between the forces acting on the robot and its kinematics. The dynamics of the robots can be divided into two main categories:

Forward dynamics: which is to determine the robot motion once the acting forces are given, and

Inverse dynamics: which evaluate the actuating joints forces for a given state of the robot position, velocity, and acceleration.

The solution of the dynamics of the robots is essential to design the components of the robots and estimating the actuators power. Moreover, when fast operation is expected or in case of heavy loaded robots it is better to establish the control algorithm based on the dynamic model. However the use of the dynamic model for the control of the robot would lead to some issues due to the complexity of the dynamics of the parallel robots. Also, the control of the parallel robots based on the dynamic model need the solution of the direct kinematics, which is quiet cumbersome itself. Thus, an important factor for providing a dynamic method is the computation time. There have been many formalisms proposed to establish the dynamics relation of the parallel robots, which in generality are equivalent, however, the challenge is to reduce the computation time and cost.

In order to determine the solution algorithm for the parallel manipulators there are two common methods to deal with their closed loop kinematic chains: one is to open the loops at certain passive links and introduce the cut joints constraints with Lagrange multipliers and apply the recursive scheme of the cut loops [19]. The other method is to use the geometrical constraints of the closed loop chain to relate the passive joints with the actuated joins, and then derive the equation of motion for the kinematic chain based on different approaches such as the Newton-Euler [20] [21], Lagrange formalism [22] [23], or even in some case the formalism can be mixed [24].

We would point the complexity of the relations of the dynamic of the 6-PUS Hexaglide mechanism based on the Newton-Euler approach for parallel robots described by Merlet [7].

3.1 Description of the dynamic model

The parameters used in the dynamic model relations are given in table 3.1 based on figure 3.1. We have used the same notation of the inverse kinematic chapter with some new parameters introduced to define the dynamic relations.

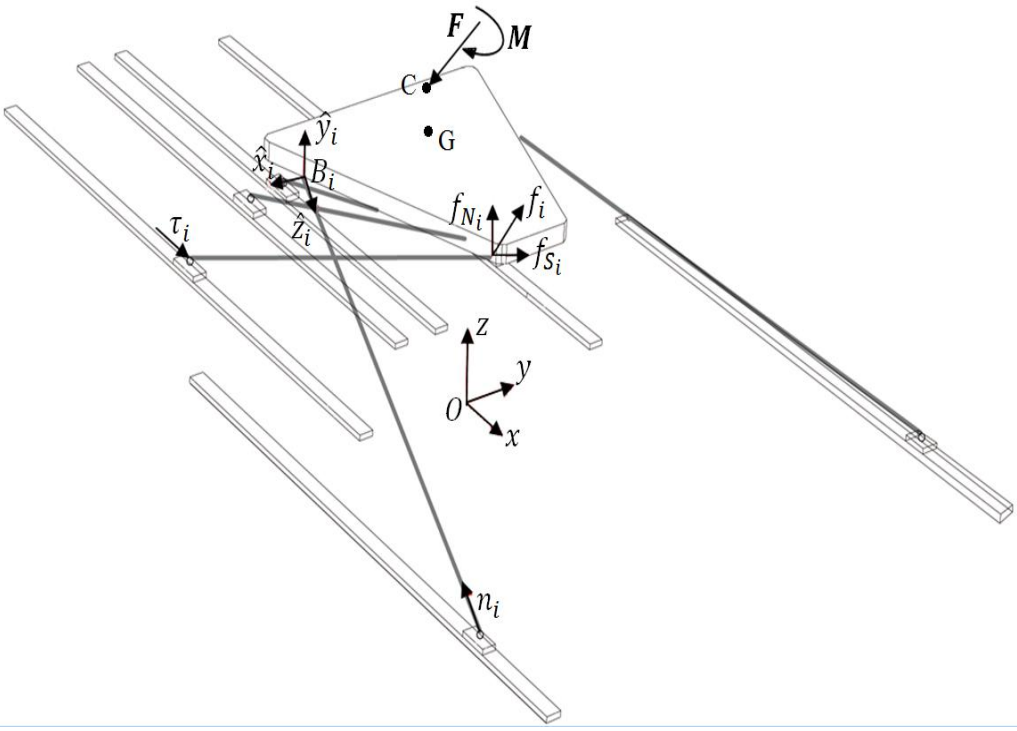

Figure 3-1 External and joint action forces applied on the robot

symbol	Description
$O-xyz$	reference fixed frame attached to the base
$C-x'y'z'$	moving frame attached to the platform
$B_i - \hat{x}_i\hat{y}_i\hat{z}_i$	local frame attached to the point B_i with $\hat{z}_i$along the direction of each link
G	center of mass of the platform
GC'	position vector from center of mass G to the TCP, projected in the local frame of platform $C-x'y'z'$
GC	position vector from center of mass G to the TCP, projected in the fixed reference frame $O-xyz$
m	mass of the platform
$\boldsymbol{I}$	inertia matrix of the platform
$J_i \equiv I_{\hat{x}\hat{x}} = I_{\hat{y}\hat{y}}$	mass moment of inertia of individual link with respect to the frame with frame $B - \hat{x}\hat{y}\hat{z}$
$\boldsymbol{F} = [F_x \quad F_y \quad F_z]^T$	force applied to the TCP of platform
$\boldsymbol{M} = [M_x \quad M_y \quad M_z]^T$	torque applied to the TCP of the platform
τ_i	actuating force of each slider
$\boldsymbol{\tau} = [\tau_1 \quad \tau_2 \quad \cdots \quad \tau_6]^T$	vector of the assembly of the actuating forces of all sliders
$\boldsymbol{f_i} = [f_{i,x} \quad f_{i,y} \quad f_{i,z}]^T$	force acting on point B_i of each link
$\boldsymbol{f_{S_i}} = [f_{S_{i,x}} \quad f_{S_{i,y}} \quad f_{S_{i,z}}]^T$	component of the force acting on point B_i along the direction of each link
$\boldsymbol{f_{N_i}} = [f_{N_{i,x}} \quad f_{N_{i,y}} \quad f_{N_{i,z}}]^T$	component of the force acting on point B_i perpendicular to the direction of each link
$\boldsymbol{g} = [g_x \quad g_y \quad g_z]^T$	gravitational acceleration field
$\ddot{\boldsymbol{p}} = [\ddot{p}_x \quad \ddot{p}_y \quad \ddot{p}_z]^T$	acceleration vector of the TCP of the platform
$\boldsymbol{\gamma}_G = [\gamma_{G,x} \quad \gamma_{G,y} \quad z]^T$	acceleration vector of center of mass of platform
$\boldsymbol{\gamma}_{B_i} = [\gamma_{B_{i,x}} \quad \gamma_{B_{i,y}} \quad \gamma_{B_{i,z}}]^T$	acceleration vector of point B_i of individual link
$\dot{\boldsymbol{\omega}} = [\dot{\omega}_x \quad \dot{\omega}_y \quad \dot{\omega}_z]^T$	angular acceleration vector of the platform
$\ddot{\boldsymbol{X}} = [\ddot{\boldsymbol{p}} \quad \dot{\boldsymbol{\omega}}]^T$	twist vector of TCP of the platform

Table 3-1 Description of the parameters used in the dynamic problem

3.2 Analytic solution of dynamic problem

Considering that the legs are rather light, Merlet have made some assumption in order to simplify the model:

- The inertia matrix of each link, expressed in the frame with origin in A_i and z axis along the link is defined as:

$$I_i = \begin{bmatrix} J_i & 0 & 0 \\ 0 & J_i & 0 \\ 0 & 0 & 0 \end{bmatrix} \tag{3.1}$$

- And the mass of the links are neglected. We can also suppose that the mass of the links are distributed between the sliders and the platform.

The force $\boldsymbol{f_i}$ acting on point B_i is decomposed in two components:

- $\boldsymbol{f_{S_i}}$ directed along the link unit vector $\boldsymbol{n_i}$
- $\boldsymbol{f_{N_i}}$ normal to $\boldsymbol{n_i}$, which is due to inertia

The force along the link is related to the actuating force τ_i by:

$$\boldsymbol{f_{S_i}} = \tau_i(\boldsymbol{n_i}.\boldsymbol{u_i})\boldsymbol{n_i} \tag{3.2}$$

Where $\boldsymbol{n_i}.\boldsymbol{u_i}$ represents the dot product of vectors $\boldsymbol{u_i}$ which is the unit vector along each rail and $\boldsymbol{n_i}$ which is obtained from the solution of the inverse kinematic equation (2.16) for a given generalized coordinate of the platform. Notice that when dealing the control problem, we have to solve the direct kinematic problem to obtain $\boldsymbol{n_i}$ from position of the actuating joints.

So we have:

$$\boldsymbol{f_i} = \boldsymbol{f_{S_i}} + \boldsymbol{f_{N_i}} = \tau_i(\boldsymbol{n_i}.\boldsymbol{u_i})\boldsymbol{n_i} + \boldsymbol{f_{N_i}} \tag{3.3}$$

We indicate $\boldsymbol{F_N}$ as the resultant of the forces $\boldsymbol{f_{N_i}}$ and $\boldsymbol{M_N}$ their resultant torque about the tool center point C. if the external force and torque applied to the TCP of the platform are $\boldsymbol{F}$and $\boldsymbol{M}$ respectively, the equilibrium equations would be:

$$\boldsymbol{F} = \sum_{i=1}^{6} \tau_i (\boldsymbol{n_i}.\boldsymbol{u_i})\boldsymbol{n_i} + \boldsymbol{F_N} \tag{3.4}$$

$$\boldsymbol{M} = \sum_{i=1}^{6} \tau_i (\boldsymbol{b_i} \times \boldsymbol{n_i}) + \boldsymbol{M_N} \tag{3.5}$$

Introducing the dimension 6 vectors:

$$\boldsymbol{\sigma}_N = \begin{bmatrix} \boldsymbol{F_N} \\ \boldsymbol{M_N} \end{bmatrix} , \qquad \boldsymbol{\sigma} = \begin{bmatrix} \boldsymbol{F} \\ \boldsymbol{M} \end{bmatrix} \tag{3.6}$$

We can rewrite equations (3.4), and (3.5) as:

$$\boldsymbol{\sigma} = \boldsymbol{J}^{-T}\boldsymbol{\tau} + \boldsymbol{\sigma_N} \tag{3.7}$$

Where $\boldsymbol{\tau}$ is the dimension 6 vector containing all the actuating forces, and $\boldsymbol{J}^{-T}$ is the dimension 6×6 matrix:

$$\boldsymbol{J}^{-T} = \begin{bmatrix} (\boldsymbol{n}_1.\boldsymbol{u}_1)\boldsymbol{n}_1^T, & (\boldsymbol{n}_1.\boldsymbol{u}_1)(\boldsymbol{n}_1 \times \boldsymbol{b}_1)^T \\ (\boldsymbol{n}_2.\boldsymbol{u}_2)\boldsymbol{n}_2^T, & (\boldsymbol{n}_2.\boldsymbol{u}_2)(\boldsymbol{n}_2 \times \boldsymbol{b}_2)^T \\ & \vdots \\ (\boldsymbol{n}_6.\boldsymbol{u}_6)\boldsymbol{n}_6^T, & (\boldsymbol{n}_6.\boldsymbol{u}_6)(\boldsymbol{n}_6 \times \boldsymbol{b}_6)^T \end{bmatrix}^T \tag{3.8}$$

The torque $\boldsymbol{M}_G$ applied to the center of mass of the platform is:

$$\boldsymbol{M}_G = \boldsymbol{M} + GC \times \boldsymbol{F} \tag{3.9}$$

The Newton-Euler equations are:

$$\begin{cases} \boldsymbol{F} + m\boldsymbol{g} = m\boldsymbol{\gamma}_G \\ \boldsymbol{M}_G = \boldsymbol{I}\dot{\boldsymbol{\omega}} + \boldsymbol{\omega} \times \boldsymbol{I}\boldsymbol{\omega} \end{cases} \tag{3.10}$$

Where **I** is the dimension 3 × 3 inertia matrix of the platform, and $\dot{\boldsymbol{\omega}}$ is its vector of the angular velocity.

The acceleration of the tool center point C of the platform can be obtained from the center of the mass G acceleration:

$$\ddot{\boldsymbol{p}} = \boldsymbol{\gamma}_G + \dot{\boldsymbol{\omega}} \times GC + \boldsymbol{\omega} \times (\boldsymbol{\omega} \times GC) \tag{3.11}$$

Therefore:

$$\boldsymbol{F} + m\boldsymbol{g} = m(\ddot{\boldsymbol{p}} + \overline{GC}\dot{\boldsymbol{\omega}} + (\boldsymbol{\omega} \times GC) \times \boldsymbol{\omega}) \tag{3.12}$$

Where the dimension 3 × 3 matrix $\overline{GC}$ represent the cross product matrix associated to the vector GC. A cross product associated to the vector GC is defined as, $\overline{GC} = GC \times I_3$, such that $GC \times \dot{\boldsymbol{\omega}} = \overline{GC}\dot{\boldsymbol{\omega}}$**.** And where I_3 is the dimension 3 × 3 identity matrix.

From equations (3.9), (3.10), and (3.11) we may write:

$$\begin{aligned} \boldsymbol{M} = \boldsymbol{M}_G - GC \times \boldsymbol{F} \\ &= \boldsymbol{I}\dot{\boldsymbol{\omega}} + \boldsymbol{\omega} \times \boldsymbol{I}\boldsymbol{\omega} - GC \\ &\times (m(\ddot{\boldsymbol{p}} + \overline{GC}\dot{\boldsymbol{\omega}} + (\boldsymbol{\omega} \times GC) \times \boldsymbol{\omega}) - m\boldsymbol{g}) \\ &= (\boldsymbol{I} - m\overline{GC}^2)\dot{\boldsymbol{\omega}} - m\overline{GC}\ddot{\boldsymbol{p}} + \boldsymbol{\omega} \times \boldsymbol{I}\boldsymbol{\omega} \\ &- m\overline{GC}\big(\boldsymbol{g} + \boldsymbol{\omega} \times (\boldsymbol{\omega} \times \overline{GC})\big) \end{aligned} \tag{3.13}$$

We define $\boldsymbol{W} = (\boldsymbol{\omega} \times GC) \times \boldsymbol{\omega}$. The Newton-Euler equations for the robot can be written in matrical form as:

$$\boldsymbol{\sigma} = T_1\ddot{\boldsymbol{X}} + \boldsymbol{T_2} \tag{3.14}$$

Where $\ddot{\boldsymbol{X}}$ is the acceleration vector of the TCP of the platform, and the 6×6 dimension matrix T_1 and 3×1 vector $\boldsymbol{T_2}$ are defined as:

$$T_1 = \begin{bmatrix} mI_3 & m\overline{GC} \\ -m\overline{GC} & \boldsymbol{I} - m\overline{GC}^2 \end{bmatrix}, \quad \boldsymbol{T_2} = \begin{bmatrix} m\boldsymbol{W} - m\boldsymbol{g} \\ \boldsymbol{\omega} \times \boldsymbol{I\omega} + m\overline{GC}(\boldsymbol{W} - \boldsymbol{g}) \end{bmatrix} \tag{3.15}$$

Again I_3 is the dimension 3×3 identity matrix.

So from equations (3.7) and (3.14) we can conclude:

$$T_1\ddot{\boldsymbol{X}} + \boldsymbol{T_2} = \boldsymbol{J}^{-T}\boldsymbol{\tau} + \boldsymbol{\sigma_N} \tag{3.15}$$

This equation represent the relation between the actuators joint force and the accelerations of the platform tool center point C, also as a function of forces perpendicular to the links $\boldsymbol{\sigma_N}$. Now we just have to define the expression of the $\boldsymbol{\sigma_N}$ in the equation (3.15).

We write the expression of the acceleration of point B_i :

$$\boldsymbol{\gamma}_{B_i} = \ddot{\boldsymbol{p}} + \dot{\boldsymbol{\omega}} \times \boldsymbol{b_i} + \boldsymbol{\omega} \times (\boldsymbol{\omega} \times \boldsymbol{b_i}) \tag{3.16}$$

Which we can write this expression in matrical form as:

$$\boldsymbol{\gamma}_{B_i} = U_{1_i}\ddot{\boldsymbol{X}} + \boldsymbol{U_{2_i}} \tag{3.17}$$

Where the 3×6 matrixe U_{1_i} and dimension 3 vector $\boldsymbol{U_{2_i}}$ are:

$$U_{1_i} = [I_3 \quad -\overline{\boldsymbol{b_i}}], \qquad \boldsymbol{U_{2_i}} = \boldsymbol{\omega} \times (\boldsymbol{\omega} \times \boldsymbol{b_i}) \tag{3.18}$$

Where $\overline{\boldsymbol{b_i}}$ is the matrix of cross product associated to vector $\boldsymbol{b_i}$.

The vector $\boldsymbol{\gamma}_{NB_i}$ which is the projection of the acceleration of point B_i on the plane perpendicular to the unit vector of the link $\boldsymbol{n_i}$ is:

$$\boldsymbol{\gamma}_{NB_i} = (\boldsymbol{n_i} \times \boldsymbol{\gamma}_{B_i}) \times \boldsymbol{n_i} \tag{3.19}$$

Which from equation (3.17) can also be written in matrical form as:

$$\boldsymbol{\gamma}_{NB_i} = -\overline{\boldsymbol{n}}_{\boldsymbol{i}}{}^2 U_{1_i} \ddot{\boldsymbol{X}} - \overline{\boldsymbol{n}}_{\boldsymbol{i}}{}^2 \boldsymbol{U}_{\boldsymbol{2_i}} \tag{3.20}$$

Besides, for each link we have:

$$\boldsymbol{f}_{\boldsymbol{N_i}} = -3\frac{J_i}{l_i{}^2}\boldsymbol{\gamma}_{NB_i} \tag{3.21}$$

The components of the vector $\boldsymbol{\sigma}_{\boldsymbol{N}}$ are:

$$\boldsymbol{F}_{\boldsymbol{N}} = \sum_{i=1}^{6} \boldsymbol{f}_{\boldsymbol{N_i}} \quad , \qquad \boldsymbol{M}_{\boldsymbol{N}} = \sum_{i=1}^{6} \boldsymbol{b_i} \times \boldsymbol{f}_{\boldsymbol{N_i}} \tag{3.22}$$

From equations (3.20), and (3.21) we can rewrite these expressions as:

$$\boldsymbol{F}_{\boldsymbol{N}} = \left(\sum_{i=1}^{6} 3\frac{J_i}{l_i{}^2}\overline{\boldsymbol{n}}_{\boldsymbol{i}}{}^2 U_{1_i}\right)\ddot{\boldsymbol{X}} + \sum_{i=1}^{6} 3\frac{J_i}{l_i{}^2}\overline{\boldsymbol{n}}_{\boldsymbol{i}}{}^2 \boldsymbol{U}_{\boldsymbol{2_i}} \tag{3.23}$$

$$\boldsymbol{M}_{\boldsymbol{N}} = \left(\sum_{i=1}^{6} 3\frac{J_i}{l_i{}^2}\overline{\boldsymbol{b}}_{\boldsymbol{i}}\overline{\boldsymbol{n}}_{\boldsymbol{i}}{}^2 U_{1_i}\right)\ddot{\boldsymbol{X}} + \sum_{i=1}^{6} 3\frac{J_i}{l_i{}^2}\overline{\boldsymbol{b}}_{\boldsymbol{i}}\overline{\boldsymbol{n}}_{\boldsymbol{i}}{}^2 \boldsymbol{U}_{\boldsymbol{2_i}} \tag{3.24}$$

Combining these two equations we can write the expression of $\boldsymbol{\sigma}_{\boldsymbol{N}}$ in matrical form as:

$$\boldsymbol{\sigma}_{\boldsymbol{N}} = V_1\ddot{\boldsymbol{X}} + \boldsymbol{V}_2 \tag{3.25}$$

Where the 6×6 dimension matrix $\boldsymbol{V}_1$and the dimension 6 vector $\boldsymbol{V}_2$ are:

$$V_1 = \begin{bmatrix} \sum_{i=1}^{6} 3\frac{J_i}{{l_i}^2}\overline{\boldsymbol{n}_i}^2 U_{1_i} \\ \sum_{i=1}^{6} 3\frac{J_i}{{l_i}^2}\overline{\boldsymbol{b}_i}\overline{\boldsymbol{n}_i}^2 U_{1_i} \end{bmatrix}, \quad \boldsymbol{V_2} = \begin{bmatrix} \sum_{i=1}^{6} 3\frac{J_i}{{l_i}^2}\overline{\boldsymbol{n}_i}^2 \boldsymbol{U_{2_i}} \\ \sum_{i=1}^{6} 3\frac{J_i}{{l_i}^2}\overline{\boldsymbol{b}_i}\overline{\boldsymbol{n}_i}^2 \boldsymbol{U_{2_i}} \end{bmatrix} \tag{3.26}$$

Now we can rewrite the equation (3.15) as:

$$(T_1 - V_1)\ddot{\boldsymbol{X}} + (\boldsymbol{T_2} - \boldsymbol{V_2}) = \boldsymbol{J}^{-T}\boldsymbol{\tau} \tag{3.27}$$

We can finally write the expression of the end-effector acceleration as a function of the actuators force, which represents the forward dynamic problem as:

$$\ddot{\boldsymbol{X}} = (T_1 - V_1)^{-1}\boldsymbol{J}^{-T}\boldsymbol{\tau} - (T_1 - V_1)^{-1}(\boldsymbol{T_2} - \boldsymbol{V_2}) \tag{3.28}$$

Then the solution of the Inverse dynamic problem of the 6-PUS Hexaglide mechanism, which is essential for the estimation of the actuators power and constructing a control algorithm, can be written as:

$$\boldsymbol{\tau} = \boldsymbol{J}^T(T_1 - V_1)\ddot{\boldsymbol{X}} + \boldsymbol{J}^T(\boldsymbol{T_2} - \boldsymbol{V_2}) \tag{3.29}$$

To design the mechanical components of the mechanism, we need to solve the inverse dynamic algorithm, which as mentioned is composed by many steps. For a given set of objectives of the end-effector generalized coordinates of position, velocity, and acceleration, we must evaluate the actuating forces and also forces in other components. We can summarize the steps of inverse dynamic analysis for the problem of the mechanical design of the mechanism as follows:

1- Solve the inverse kinematic problem, and determine the actuators joint coordinate $\boldsymbol{\lambda} = [\lambda_1 \quad \lambda_2 \quad \dots \quad \lambda_6]^T$, and consequently evaluate the unit vectors along the direction of each link $\boldsymbol{n_i} = [n_{i,x} \quad n_{i,y} \quad n_{i,z}]^T$ from equation (2.16).

2- Evaluate the vector GC from the relation $GC = RGC'$, and consequently the associated cross product matrix $\overline{GC}$.

3- From the equation(3.15), determine the matrix T_1, and vector $\boldsymbol{T_2}$ using vector of the angular velocity of the platform $\boldsymbol{\omega} = [\omega_x \quad \omega_y \quad \omega_z]^T$

4- Again using the orientation of the platform evaluate vector $\boldsymbol{b_i} = R\boldsymbol{b_i'}$, and consequently the associated cross product matrix $\overline{\boldsymbol{b}}_{\boldsymbol{i}}$.

5- Evaluate matrix U_{1_i} and vector $\boldsymbol{U_{2_i}}$ from equation (3.18)

6- Using the expression of the unit vectors along link which is obtained from inverse kinematic, evaluate the matrix V_1 and vector $\boldsymbol{V}_2$ from equation (3.26)

7- Calculate the matrix $\boldsymbol{J}^{-T}$ from equation (3.8), and the $\boldsymbol{J}^T$ through numerical inversion, keeping in mind that the unit vector along each rail is $\boldsymbol{u_i} = [1 \quad 0 \quad 0]$.

8- Finally, define the actuators forces $\boldsymbol{\tau}$ from equation (3.29)

However, when dealing with the control problem using the inverse dynamic, the procedure would be more complex. In the control problem we will face the direct kinematic instead of the inverse kinematic, which leads to more complexity. The first step is to measure the actuating joints parameters λ_i , and then from the solution of the direct kinematic find the pose and orientation of the end-effector, and consequently the velocity and acceleration. Then applying steps 2 to 8, we can determine the actuating force. However, despite the serial mechanisms, in parallel robots the direct kinematic problem is much more complex than the inverse one. This will lead to higher computation time which would lead to trouble in real time control. That's why the use of the dynamic equations for the control loop of the parallel robots in practice is limited. M. Honegger, A. Codourey, E. Burdet[25],

have proposed a non-linear adaptive control method based on the dynamic equations for the Hexaglide manipulator. The minimization of the tracking errors are used online to correct the parameters used in the dynamic equations.

3.3 Simulation

There are many different multi body dynamics software, that can be applied to solve the dynamic problem of the Hexaglide. In order to create the dynamic model of the mechanism, we have applied Adams multi body dynamics software. Adams is considered as the most famous and widely used MBD software to study the motion of the rigid bodies, which could run nonlinear dynamics in a fraction of the time required by FEA solutions. Loads and forces computed by Adams simulations improve the accuracy of FEA by providing better assessment of how they vary throughout a full range of motion and operating environments and allow different loading combination to be studied.

Another advantage is its multidiscipline solution, which can be used with different modulus available to integrate mechanical components, pneumatics, hydraulics, electronics, and control systems technologies to build and test virtual prototypes that accurately account for the interactions between these subsystems. For instance Adams/Mechatronics is a plug-in to Adams which can be used to incorporate control systems into mechanical models.

To solve the inverse dynamic of the robot in Adams, we must do the following steps:

3.3.1 Create geometry

First step is to create the geometry of the model and introduce the proper set of constraints between the bodies by creating the prismatic, universal, and spherical joints for each kinematic chain. The material properties of each rigid body must be also defined, for the evaluation of the mass and inertia.

The geometric parameters of the mechanism under study are given in table.2.2 in the inverse kinematic chapter. These geometric data are given when the sliding actuators are at their initial position.

The geometries for the mechanism architecture are proposed by the multi objective optimization done before. The objectives of the optimization method are: coverage of the desired workspace, minimization of multiplication of the forces and torques applied on the TCP in the static condition and transmitted along the links, the longitudinal size, and the interference between the links.

At the first stage, we have created a rough model based on these geometric data in Adams, to perform the simulation and discuss some aspects of the dynamic of the robot. After, in the chapter 4, we will provide the detailed CAD model of the mechanism, and we will develop the results of the dynamic simulation on the precise model.

The mass and inertia properties of the components are given in table 3.2. We have exported these values for the rough model from Adams.

Mass of the legs $l_i[kg]$	$m_{l_1} = m_{l_6} = 1.69$ $m_{l_2} = m_{l_4} = 1.96$ $m_{l_3} = m_{l_5} = 1.74$
Inertia tensor of each link about$L_i - \check{x}_i\check{y}_i\check{z}_i$ *$[kg - m^2]$	$I_{l_1} = I_{l_6} = diag[0.22 \quad 0.22 \quad 3.3e-4]$ $I_{l_2} = I_{l_5} = diag[0.33 \quad 0.33 \quad 3.8e-4]$ $I_{l_3} = I_{l_4} = diag[0.23 \quad 0.23 \quad 3.4e-4]$
Mass of platform $[kg]$ Inertia tensor of the platform about its centrodial axes $[kg - m^2]$	$m = 35$ $\boldsymbol{I} = diag[0.89 \quad 1.57 \quad 2.43]$
Mass of sliders $[kg]$	$m_{s_1} = m_{s_2} = \cdots = m_{s_6} = 8$
Gravitational acceleration $[m/s^2]$	$\boldsymbol{g} = [0 \quad 0 \quad -9.81]^T$
* $L_i - \check{x}_i\check{y}_i\check{z}_i$ is the local coordinate at the center of the mass of each link with $\check{z}_i$ along the links axis	

Table 3-2 Mass and inertia properties of the mechanism

3.3.2 Simulation with TCP imposed motion

In order to evaluate the dynamics of the mechanism for a given motion of the TCP, first it is necessary to solve the inverse kinematic problem by performing a simulation with the imposed motion of the TCP and derive the time history of the actuated joints coordinates – prismatic joints displacement – during the motion of the platform. To do that the following steps must be done:

- Introduce the desired motion law to the TCP of the platform
- Create state variables to store the numeric set of data for displacement of each prismatic joint during the motion simulation
- Perform the simulation with the given time of the TCP motion law.

3.3.3 Simulation with prismatic joints imposed motion

After performing the simulation with the defined motion of the TCP of the platform, and determining the actuated joints coordinate, another simulation must be performed by imposing the evaluated actuators displacements.

The motion law of the actuators -Prismatic joints- is defined through mathematical interpolation of the numeric set of data of the displacement of the prismatic joints which are stored in the state variables. In Adams it is possible to create splines from two independent coordinate by different methods. Here, the cubic curve fitting method is applied to create the spline for the set of actuators displacements numeric data and the time vector of the simulation.

Final step is to impose the defined motion law to each sliding joint, and remove the imposed motion of the TCP, and run a new simulation for a given time of the sliding joints motion law.

After running the simulation we can manipulate the Adams post processor for data analyzing

3.4 Discussion of the links mass and inertia

First we will discuss about the effect of the inertia and mass of each links, in the solution of the inverse dynamic problem. We will perform the simulation for a generic motion law, with different consideration of the mass and inertia of the links.

In the analytic model for the dynamic problem that we mentioned, the mass of the links have been neglected. Also the terms related to the inertia of the legs correspond to the axis along the link direction have been neglected. In Adams, we don't need to remove any parameter. However, we will show that the effects of these terms are not significant.

We have performed the simulation for the motion law given in table 3.3 imposed to the TCP of the platform.

TCP Motion law : $f = 0.7\ [Hz]$			
$x(t)\ [m]$	$0.5\sin(2\pi f.t)$	$\alpha(t)\ [deg]$	0
$y(t)\ [m]$	0	$\beta(t)\ [deg]$	0
$z(t)\ [m]$	z_{TCP}	$\gamma(t)\ [deg]$	0

Table 3-3 Motion law of the TCP for the dynamic simulation

Figure 3.3 Show the magnitude of the force evaluated in the universal joint connecting the first slider to the link, for three different cases. In the first case we don't neglect any term. Then we neglect the term $I_{\hat{z}\hat{z}}$ in the inertia tensor and the mass of the link. It can be seen that there is not a significant change in the results. Figure 3.4 shows the same results for the spherical joint connecting the leg to the platform for the first kinematic chain.

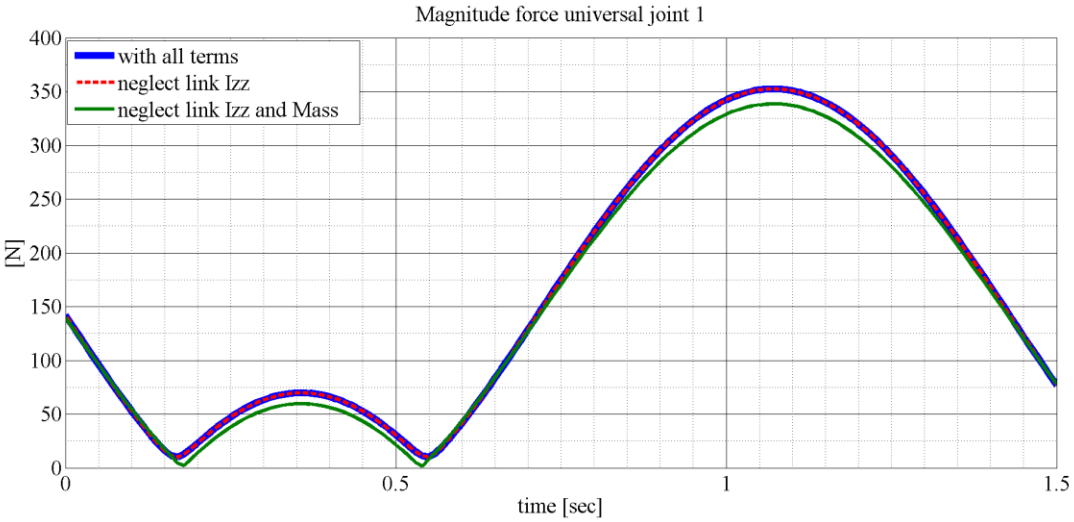

Figure 3-2 effect of mass and inertia on the magnitude force of the universal joint of the first kinematic chain

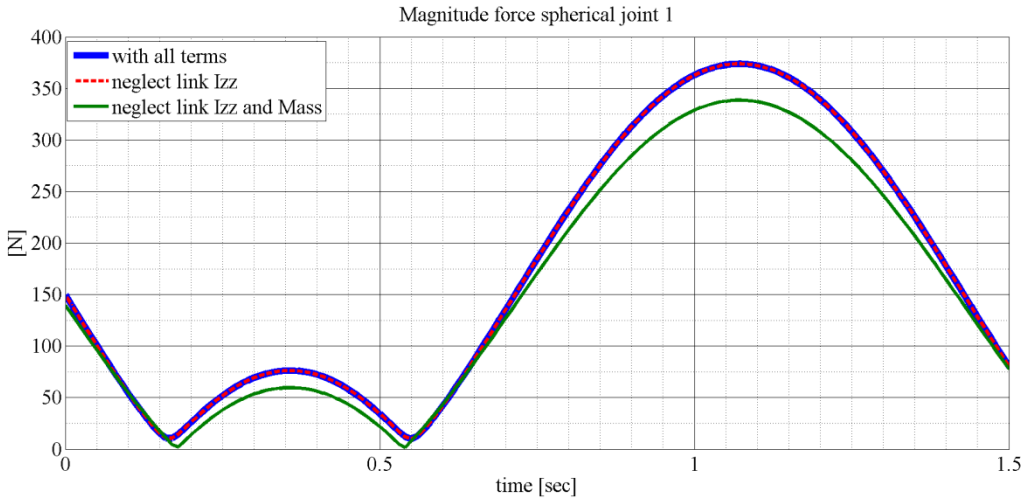

Figure 3-3 effect of mass and inertia on the magnitude force of the spherical joint of the first kinematic chain

Also we can see in figure3.5 that even when the mass and inertia terms of the links are not neglected, the components of the force in the universal joint perpendicular to the axis along the link direction, which are due to the inertia of the leg are negligible. The only difference in the trend of the curve is due to the fact that in figure 3.3 we evaluate the magnitude of the force. This result can be used to determine the forces in the legs. Since we can neglect the effect of the mass and inertia of the links, we can consider it as a two-force element. So the force in the links can be properly estimated through the forces in the universal or spherical joint.

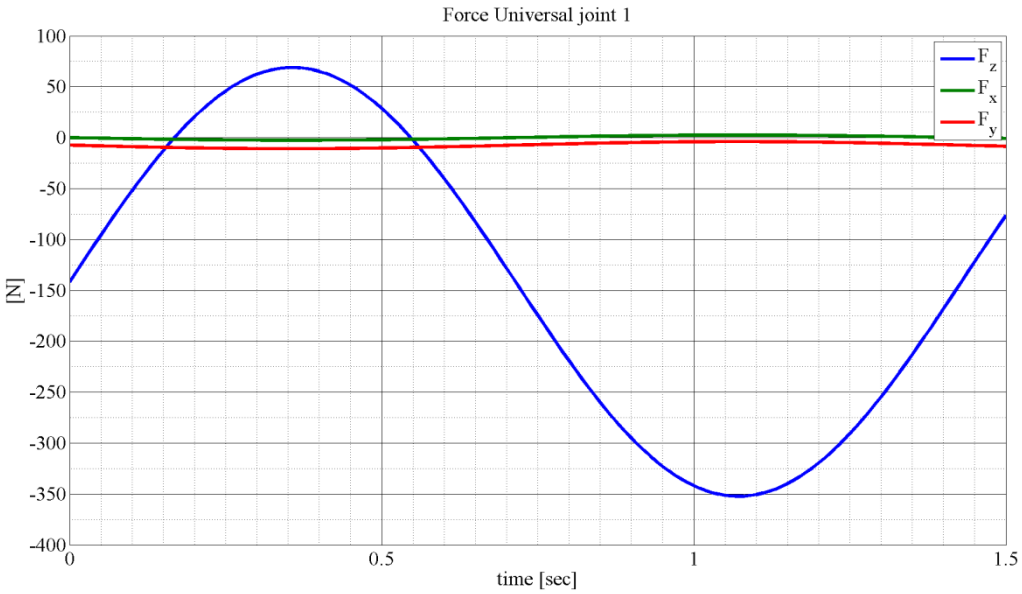

Figure 3-4 Components of force of the universal joint of the first kinematic chain, projected to the local frame with z axis along the link

Since Adams considers all the components as rigid body we can't evaluate the forces in the links. One solution is to use other software such as MSc Nastran which is able to perform dynamic analysis of the flexible bodies. However it seems to be unnecessary. Figure 3.6 shows the magnitude of the forces for the universal joint and the spherical joint of the first kinematic chain together without neglecting the mass and inertia terms. It can be seen that the forces in the universal joint and the

spherical one at the two ends of the leg are not exactly equal. But still we can use these values with a proper safety factor to design the legs. In this estimation, we not only neglect the inertia and weight force related to the mass of the link but also the effect of all the terms in inertia tensor are neglected.

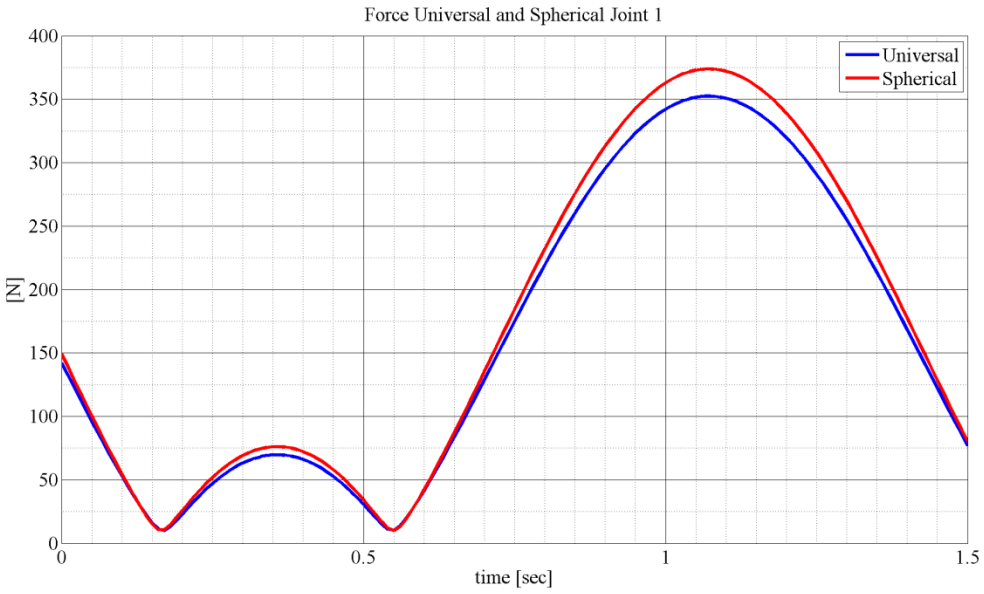

Figure 3-5 Magnitude force of the universal and spherical joint of the first kinematic chain

.

Chapter 4 Design

In order to design the mechanical components, we need to have a sense of the dynamic of the robots, in its working condition inside the desired workspace. We have used the method of dividing the workspace into a grid of points. Then for the TCP positioned at each point of this grid different combination of movements to the TCP have been imposed, and simulation to realize the dynamic of the mechanism is done. However, to apply this method it is necessary to perform a huge number of simulations.

4.1 Work space definition

In figure 4.1 a scheme of the robot when the TCP is at its home position, and the projection of desired workspace in xz and yz planes is represented. At the home position the platform has no orientation respect to the reference frame and its position coordinate of TCP is defined as $\boldsymbol{p} = [0 \quad 0 \quad z_{TCP,0}]^T$, and the mechanism architecture is designed so that in the home position the axes of the joints at A_i and B_i are along the direction of the links.

One great advantage of the parallel manipulators based on Hexaglide architecture compared to other 6dof parallel mechanism is in term of their workspace. Since all the rails are horizontal with respect to the fixed reference frame, it is possible to easily extend the workspace along the x direction by increasing the length of the links. The robot is capable to cover all the points in the yz plane of workspace along the x direction only by a pure displacement of the whole mechanism along the rails.

We aim to realize the dynamics of the robot for its working condition of TCP inside the desired work space. In particular we divide the desired works space of the TCP of the robot in the yz plane into a grid of 17×17 points. At each point of this grid various motion laws described in table 4.1 are imposed and all the steps described in the dynamic chapter, to solve the inverse dynamic problem are performed.

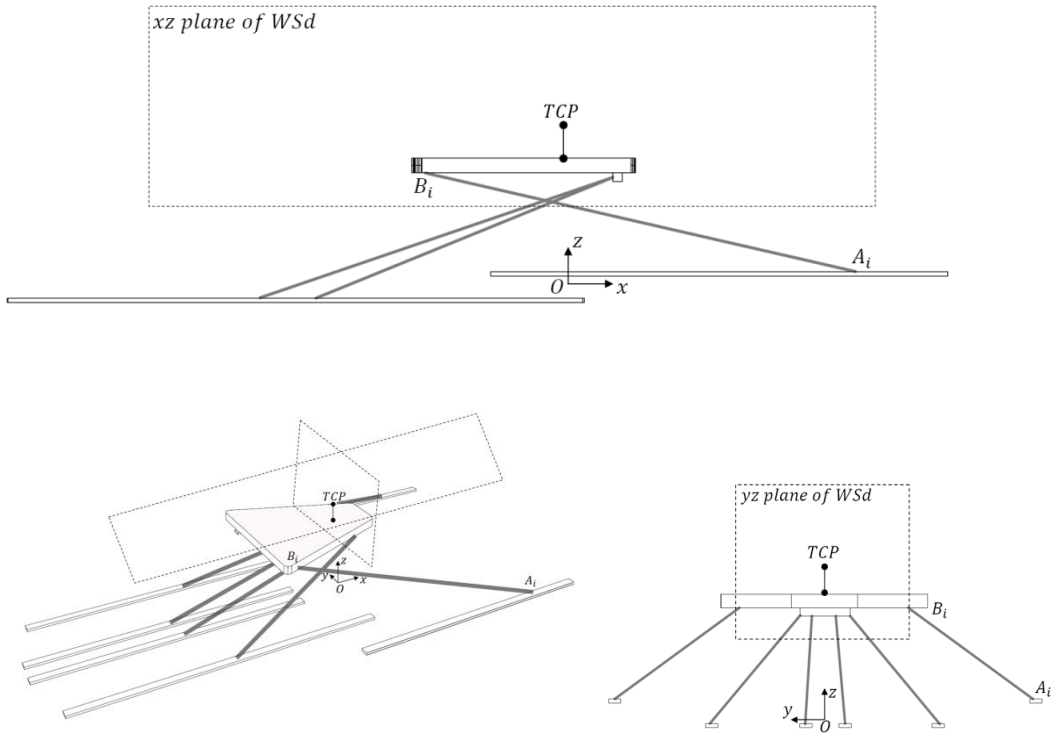

Figure 4-1 Description of the workspace of the robot

4.2 Description of the motion laws of TCP

For each single coordinate of the TCP of the platform$\boldsymbol{X} = [x \quad y \quad z \quad \alpha \quad \beta \quad \gamma]^T$, a sinusoidal motion is imposed separately, at every point in the grid inside the desired work space. At any point of the working grid all the combination of three set of orientation $\{-15°, 0°, +15°\}$ for each angle of the localframe of the platform with respect to the fixed reference frame are considered. Based on the sinusoidal motion defined in equation 4.1 all the 6 different motion laws are represented in table 4.1.

$$\begin{cases} x = A_{0,x} + A_x \sin(2\pi f t) \\ y = A_{0,y} + A_y \sin(2\pi f t) \\ z = A_{0,z} + A_z \sin(2\pi f t) \\ \alpha = A_{0,\alpha} + A_\alpha \sin(2\pi f t) \\ \beta = A_{0,\beta} + A_\beta \sin(2\pi f t) \\ \gamma = A_{0,\gamma} + A_\gamma \sin(2\pi f t) \end{cases} \quad (4.1)$$

	$x(t)\ [m]$		$y(t)\ [m]$		$z(t)\ [m]$	
	$A_{0,x}$	A_x	$A_{0,y}$	A_y	$A_{0,z}$	A_z
1)$mov.x$	0	0.5	$y_{WSd,-} \div y_{WSd,+}$	0	$z_{WSd,-} \div z_{WSd,+}$	0
2)$mov.y$	0	0	0	$\frac{1}{2}L_{WSd,y}$	$z_{WSd,-} \div z_{WSd,+}$	0
3)$mov.z$	0	0	$y_{WSd,-} \div y_{WSd,+}$	0	0	$\frac{1}{2}L_{WSd,z}$
4)$mov.\alpha$	0	0	$y_{WSd,-} \div y_{WSd,+}$	0	$z_{WSd,-} \div z_{WSd,+}$	0
5)$mov.\beta$	0	0	$y_{WSd,-} \div y_{WSd,+}$	0	$z_{WSd,-} \div z_{WSd,+}$	0
6)$mov.\gamma$	0	0	$y_{WSd,-} \div y_{WSd,+}$	0	$z_{WSd,-} \div z_{WSd,+}$	0
	$\alpha(t)\ [deg]$		$\beta(t)\ [deg]$		$\gamma(t)\ [deg]$	
	$A_{0,\alpha}$	A_α	$A_{0,\beta}$	A_β	$A_{0,\gamma}$	A_γ
1)$mov.x$	$-15 \div 15$	0	$-15 \div 15$	0	$-15 \div 15$	0
2)$mov.y$	$-15 \div 15$	0	$-15 \div 15$	0	$-15 \div 15$	0
3)$mov.z$	$-15 \div 15$	0	$-15 \div 15$	0	$-15 \div 15$	0
4)$mov.\alpha$	0	15	$-15 \div 15$	0	$-15 \div 15$	0
5)$mov.\beta$	$-15 \div 15$	0	0	15	$-15 \div 15$	0
6)$mov.\gamma$	$-15 \div 15$	0	$-15 \div 15$	0	0	15

Table 4-1 description of the motion laws applied to the TCP

$$y_{WSd,-} = -\tfrac{1}{2}L_{WSd,y} \quad , \quad y_{WSd,+} = +\tfrac{1}{2}L_{WSd,y}$$

$$z_{WSd,-} = z_{TCP,0} - \tfrac{1}{2}L_{WSd,z} \quad , \quad z_{WSd,+} = z_{TCP,0} + \tfrac{1}{2}L_{WSd,z}$$

Notice that the frequency f and the amplitude A of the sinusoidal motions are chosen to simulate the motion as similar as possible to the practical application. For example in case of simulating the real working condition of the offshore wind turbine we considered the frequency of the motion equal to $0.7\ [Hz]$. The average values of the motion A_0 are prescribed so that covers all the possible ranges inside the desired workspace.

4.3 Description of the method of automating simulations

As mentioned before, in order to realize the dynamics of the mechanism it is necessary to perform a huge number of simulations with different motion laws at each point of the WSd. In Adams, there is the possibility of automating the work by using Macros. A macro is a single command that is created to execute a series of Adams/View commands. It is possible to write the commands that the macro executes using the Adams/View command language. Adams treats a macro as it does all other Adams/View commands. Once the macro is created, we can execute it to automate the repetitive procedures. Figure 4.2 represents an example of macro which is composed to automate the simulation of the 4^{th} case of motion of the TCP described in table 4.1 : 4)mov.α.

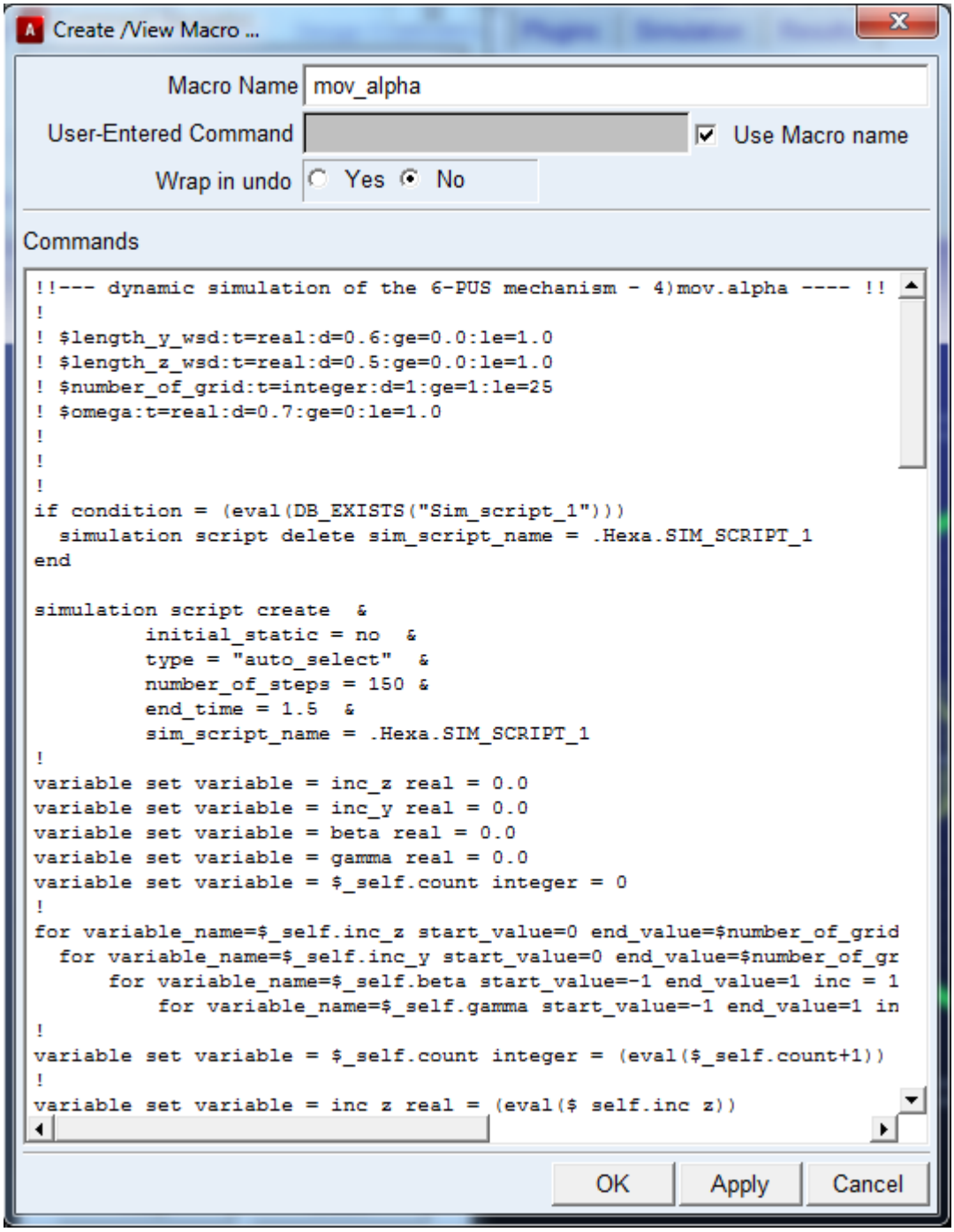

Figure 4-2 Macro command to execute the simulations of motion law 4) mov.α

Since the drawing capabilities of Adams/view are not so elevated, in order to perform proper simulations, first the precise geometries of the mechanism using CAD software are created. Then the model is imported in *.xmt extension into Adams/View with accurate geometries, and the necessary steps of the dynamic analysis are applied on this model. In figure 4.3 the imported model of the mechanism is represented.

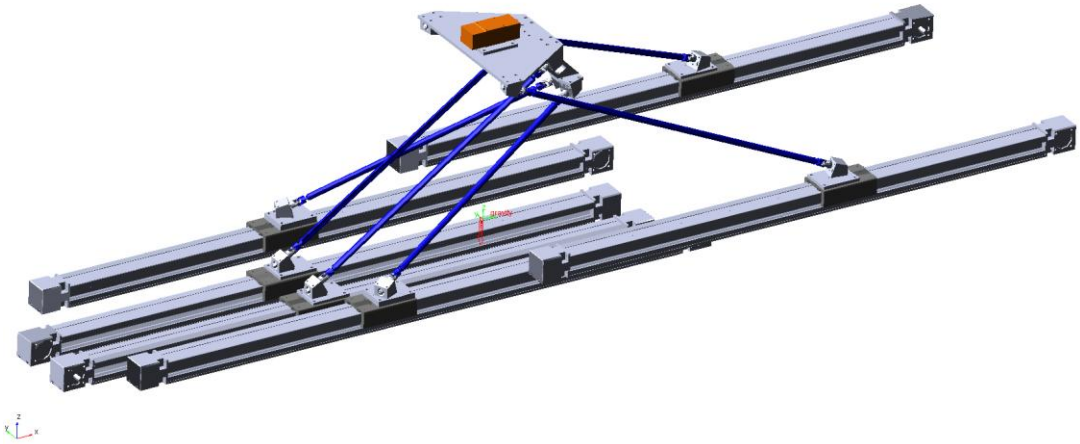

Figure 4-3 geometry of the model imported inside Adams

However the imported model consists of too many bodies that must be connected to each other by introducing proper constraints. This leads to increase the load of data to be executed at each single simulation. Furthermore, when, the macro is executed, Adams performs the simulations automatically, and for each simulation a set of results are saved. In each set of result a huge number of data are saved, including the three components of the forces and torques, and also the displacements and orientation of each joint and all the rigid bodies with respect to the reference frame. These data can be explored after the simulations finish by the post processer. However, as the automatic procedure go on and the number of simulations increase, the amount of data that are saved on the memory highly increase. This leads to increase continuously the execution time of the analysis drastically.

In Adams, it is possible to create Requests to ask for standard displacement, velocity, acceleration, or force and torque information that will help the

investigation of the results of the simulation. It is also possible to define other quantities such as pressure, work, energy, momentum, and more.

To solve the problem of increased execution time, it is possible to avoid saving the default results sets automatically, and then create some requests for the quantities that are more of interest, and then write the data of each request on a file on hard disk for each simulation.

Each request contains 8 fields that for each filed it is possible to define the quantity by some function expressions by manipulating the function builder in Adams. For instance the actuating force of the prismatic joints can be created in the way depicted in figure 4.4.

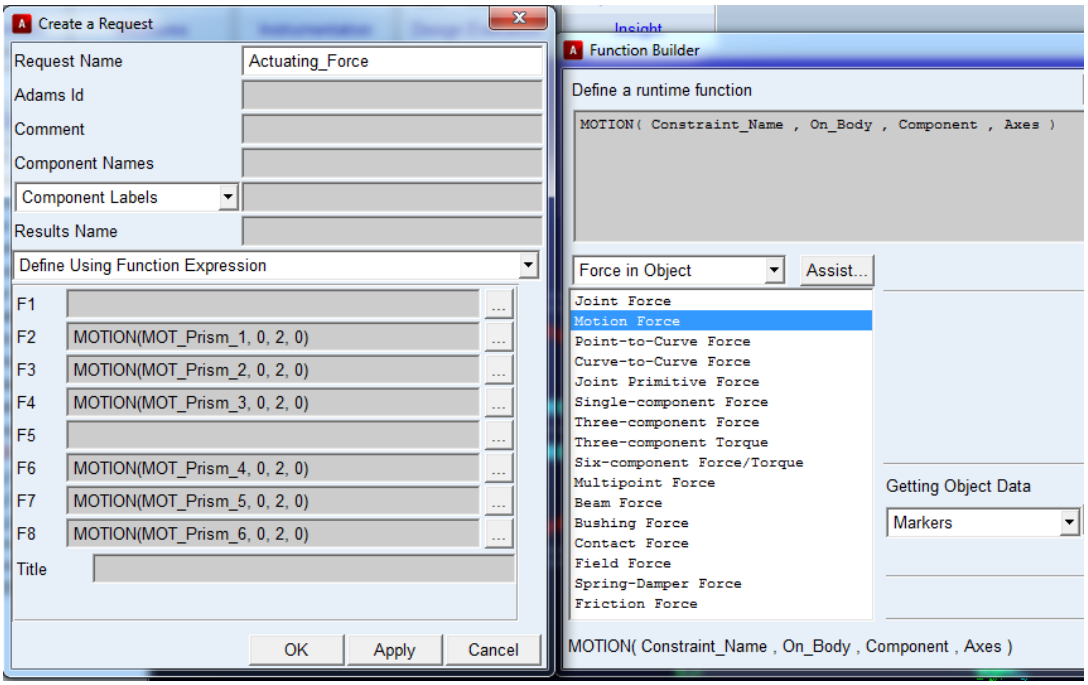

Figure 4-4 Create request to store the linear actuating force of the prismatic joints

4.4 Design Features

4.4.1 Alternative passive joints

Basically each kinematic chain of the 6-PUS parallel robot is consist of a prismatic joint on the base which is followed by the universal joint connecting the slider to the link, and the link is connected to the platform by a spherical joint. The working range of the universal and spherical joints have a significant effect on the manipulator's workspace. However, we can adapt different alternatives to design the joints. This modularity of the components is one of the advantageous characteristics of the Hexaglide manipulators in terms of mechanical construction, There are some kinematically equivalent alternative design of the joints in the platform and base that influence the properties of the manipulator.

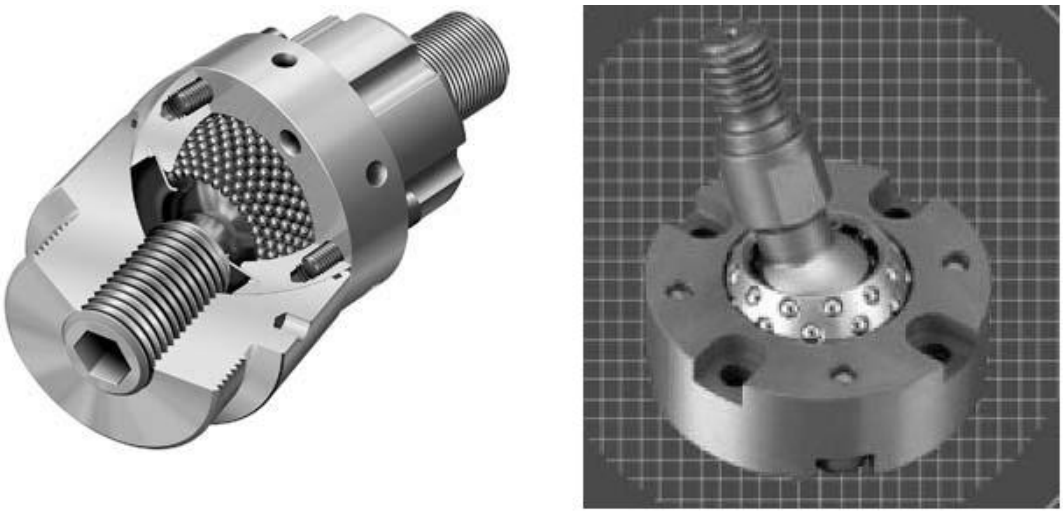

Figure 4-5 Spherical joints of INA and Hephaist Seiko (pictures courtesy of INA-Schaeffler KG and Hephaist Seiko) [7]

The spherical joint allow the three dof that represent the amount of rotation around their first reference frame's x, y and z axis and constraint the other displacement degree of freedoms. Figure 4.5 shown some typical types of ball and socket joints used in parallel architectures. However the typical spherical joints have limitation of range of mobility and it is difficult to achieve joint range of more than 30 degrees respect to the axis of symmetry passing through its center. Alternatively we can achieve the three rotational dof by different configurations. One solution is to

mount the universal joint over a revolute joint figure.4.6.c another solution is to use three revolute joints whose axes pass through the same points [10].

The universal joint allows two rotational degree of freedom around two mutually perpendicular axes, and constrains all other movements. Different universal joints of gimbals type are available with maximum misalignment angle of about 50 degrees. Figure 4.6.a shows a typical gimbals type universal joint. It is also possible to add a redundant degree of freedom in the connection of the link to the base by using the same configuration described for the spherical joint figure 4.6.c. Adding the revolute joint dof may reduce the effect of the joint range limitations.

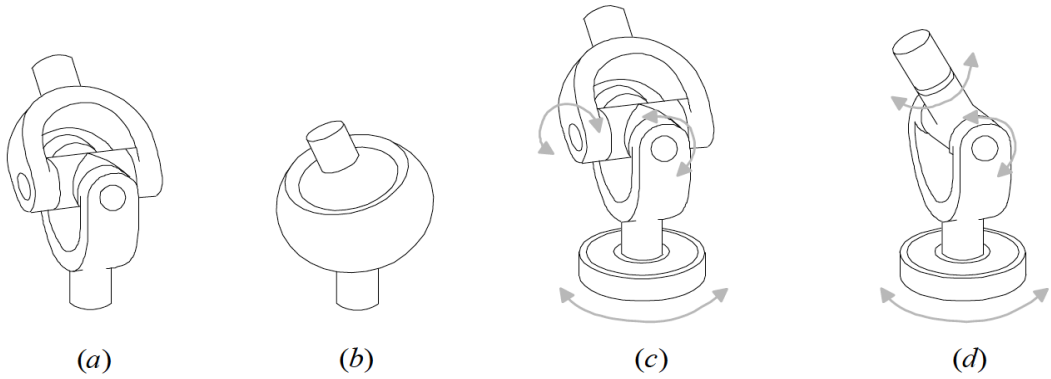

Figure 4-6 (a) The base universal joints and (b-d) three alternatives for the mobile platform spherical joints.

In our mechanism we have applied the configuration of figure 4.6.c for both the spherical equivalent joint on the platform connection and the joint connecting the link to the slider. Even with this synthesis of the kinematic chain the Grubler's formula of the mobility would result in 6 redundant degrees of the freedom, but for a proper mobility analysis of the parallel manipulators the geometrical constraints of the closed loop kinematic chain must be also considered(see appendix A).

4.4.2 Actuators design

To create the linear motion of the sliders we can apply different solutions. In general we can choose among linear motion guide actuators such as screw types

together with a rotary electric motor, or create the linear motion by a linear motor itself.

The three solutions proposed are:

- Screw transmission with or without rolling element
- Toothed belt drive
- Linear motor

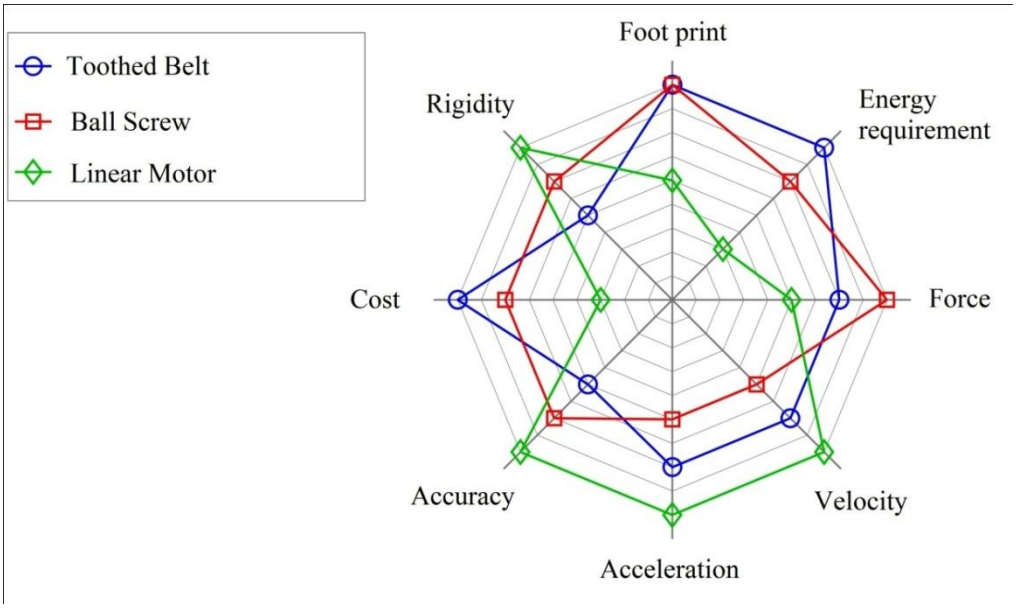

Figure 4-7 Comparison between different linear motion generators. The distant from the center indicate the convenience of the performance feature. [11]

In figure 4.7 a general comparison of technical features among the three possible solutions is represented. The decision should be taken so that best meets the technical and economic demands of the application.

Although the linear motors have great system performance in terms of fast and precise applications and good rigidity compared to other solutions it owns the disadvantage of higher footprint which require more space and also high energy consumption which consequently also leads to necessity of a complex cooling systems.

In this thesis we consider and compare in particular the ball-screw actuators figure 4.8, and the belt drive figure 4.9. They are available in various sizes and are often available both from the same manufacturer. The main advantage lies in the adoption of their accuracy and standardized technical features provided, useful for their choice and the sizing process.

Ball screw is composed of a threaded shaft which provides a helical raceway for ball bearings. With rolling elements, the ball screw drive has a very low friction coefficient and is typically greatly efficient. The forces transmitted are distributed over a large number of ball bearings, giving a low relative load per ball comparatively.

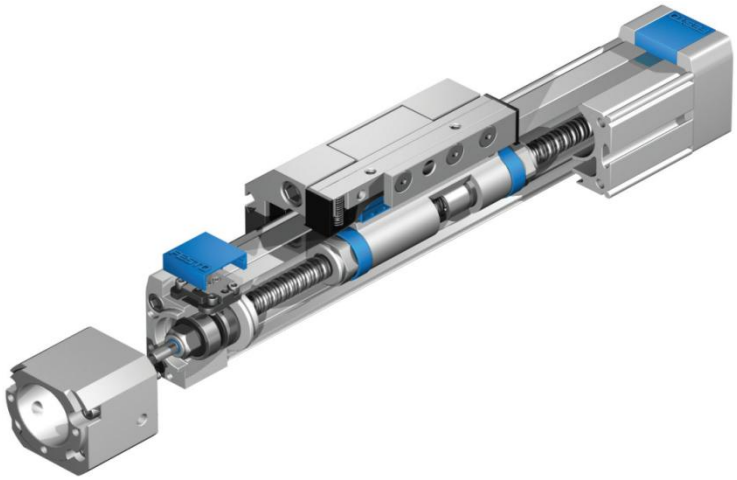

Figure 4-8 Ball screw linear actuator DGE-SP Festo

The toothed belt drive is consists of a toothed belt that runs over matching toothed pulleys. Toothed belt drives are characterized by a synchronous and slip-free power transfer while subjecting the bearing to just a small load. They are an increasingly attractive option for engineering applications as they are maintenance-free, quiet and extremely cost-effective.

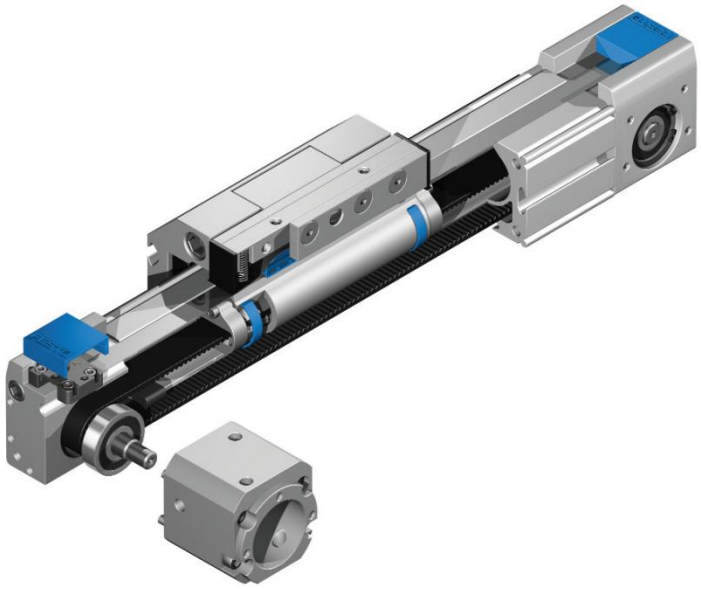

Figure 4-9 Toothed Belt drive DGE-ZR Festo

The linear actuator must be chosen so that meet the following requirements:

- The maximum stroke of the sliders:

$$\max\left(\lambda_i(t)\right) - min\left(\lambda_i(t)\right) \tag{4.2}$$

- The maximum speed and acceleration of sliders:

$$\max\left(\left|\dot{\lambda}_i(t)\right|\right)\ ,\ \ max\left|\ddot{\lambda}_i(t)\right| \tag{4.3}$$

- Maximum transmissible linear motion force:

$$max|\tau_i(t)| \tag{4.4}$$

- Maximum constraint reaction forces

$$max\left|F_{A_{i,y}}(t)\right|\ ,\ \ max\left|F_{A_{i,z}}(t)\right| \tag{4.5}$$

- Maximum constraint reaction torques

$$max\left|T_{A_{i,x}}(t)\right|,\ \ max\left|T_{A_{i,y}}(t)\right|,\ \ max\left|T_{A_{i,z}}(t)\right| \tag{4.6}$$

From the solutions of the inverse kinematic problem, we can explore the maximum value of the stroke $\lambda_i(t)$, velocity $\dot{\lambda}_i(t)$, and acceleration $\ddot{\lambda}_i(t)$ of the sliding joint. Also the components of the forces $\tau_i(t)$, $F_{A_{i,y}}(t)$, $F_{A_{i,z}}(t)$ and torques $T_{A_{i,x}}(t)$, $T_{A_{i,y}}(t)$, $T_{A_{i,z}}(t)$ are obtained from the inverse dynamic simulation for the desired motion of the platform.

4.5 Results

The calculated mass and inertia of the components based on the geometries and material properties of each component are given in table 4.2 – 4.4.

The links consist of the cylindrical bar connected to two universal joint heads at both ends. Since the material of the cylinder and the U-joint heads are the same we consider them as a whole body. And the mass and inertia properties are given in table 4.2.

The platform body is designed so that connects all the links into six bearing cases of the revolute joints without problem of interference between links and the body of the platform. We should also consider the balance which is mounted on the platform for supporting the prototype and measurement purpose. The properties of the platform together with the bearing cases and the balance are given in table 4.3.

Belt driven unit consist of the belt carriage, the bearing box, and the u-joint head. Since the sliders don't have any orientation, their inertia tensor is of no interest in the evaluations.

Links		
	Mass $[kg]$	Inertia about $L_i - \check{x}_i\check{y}_i\check{z}_i$ * $[kg{-}m^2]$
Links 1&6	2.15	$diag[0.36 \quad 0.36 \quad 3.7e-4 \ldots]$
Links 2&5	2.67	$diag[0.74 \quad 0.74 \quad 4.8e-4]$
Links 3&4	2.31	$diag[0.46 \quad 0.46 \quad 4.1e-4]$
* $L_i - \check{x}_i\check{y}_i\check{z}_i$ is the local coordinate at the center of the mass of each link with $\check{z}_i$ along the links axis		

Table 4-2 Mass and inertia properties of links

Platform	
Mass $[kg]$	Inertia about $G_i - \tilde{x}_i\tilde{y}_i\tilde{z}_i$ ** $[kg{-}m^2]$
35.84	$diag[1.36 \quad 0.88 \quad 0.71]$
** $G_i - \tilde{x}_i\tilde{y}_i\tilde{z}_i$ is the local coordinate at the center of the mass of platform	

Table 4-3 Mass and inertia properties of platform

Belt driven unit carriage	
	Mass $[kg]$
Sliders 1&6	8.01
Sliders 2&5	7.40
Sliders 3&4	7.80

Table 4-4 Mass properties of sliders

The prototype to be tested in the wind tunnel is consist of a turbine tower and the rotary unit, which is modeled as a cylinder, mounted on the TCP, and a disk connected to the cylinder in its center with an offset of 0.1 $[m]$ figure 4.10. The geometries and the mass properties of the prototype model are given in table 4.5.

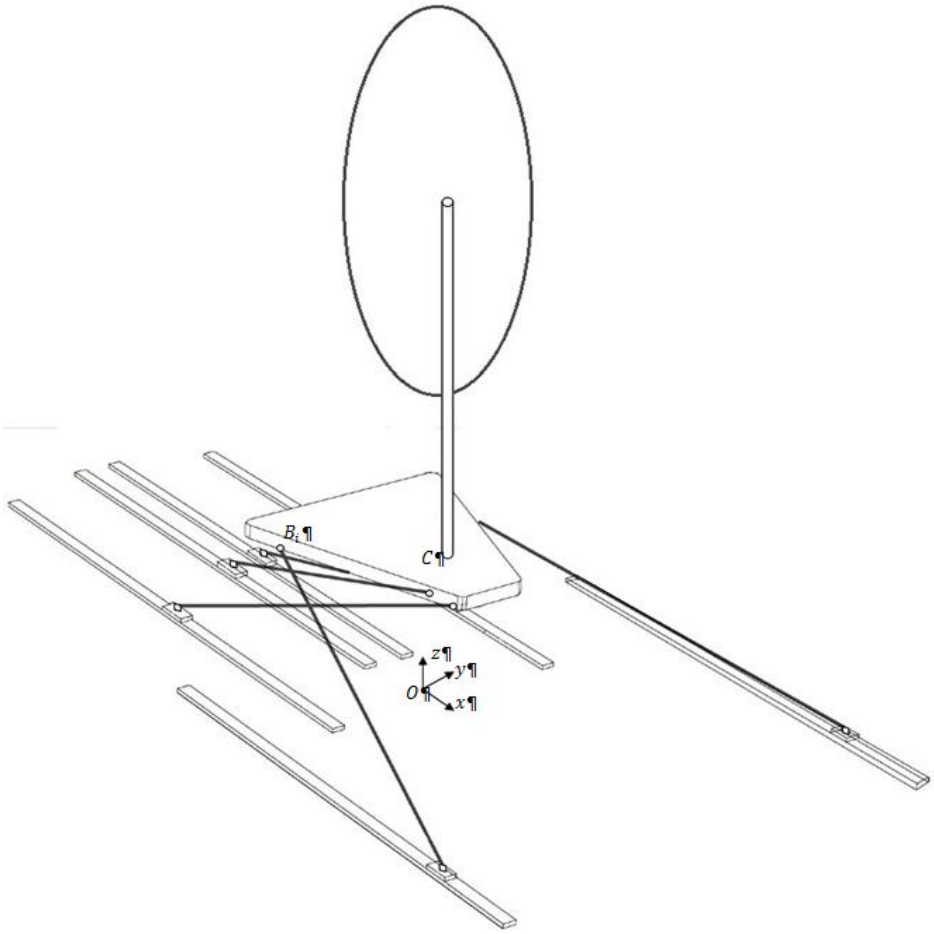

Figure 4-10 Scheme of the model of the wind generator prototype test

Wind generator prototype				
cylinder			disk	
Height $[m]$	Radius $[m]$	Mass $[kg]$	Radius $[m]$	Mass $[kg]$
1.7	0.05	7.0	1.0	3.0

Table 4-5 geometry and mass properties of the wind generator prototype

Figure 4.11– 4.13 represents the trend of actuating force of the first three kinematic chains of the mechanism for different positions of the TCP inside the desired workspace. For the case of $mov.4\ (\alpha)$ in each point of the gird inside the yz plane

of workspace 9 different combinations of the rotation angles β and γ of the platform together with a sinusoidal motion of angle α are applied and the maximum value has been plotted.

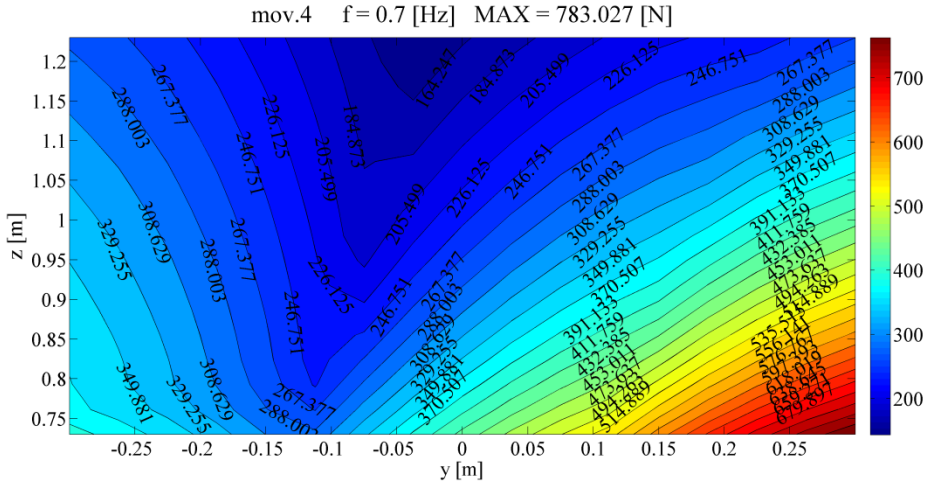

Figure 4-11 Maximum actuating force of the kinematic chain 1, motion law: 4)mov.α

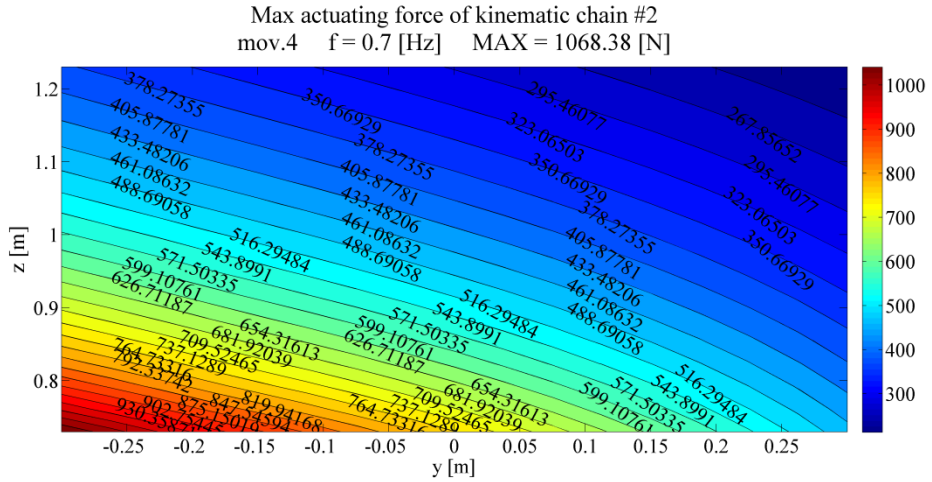

Figure 4-12 Maximum actuating force of the kinematic chain 2, motion law: 4)mov.α

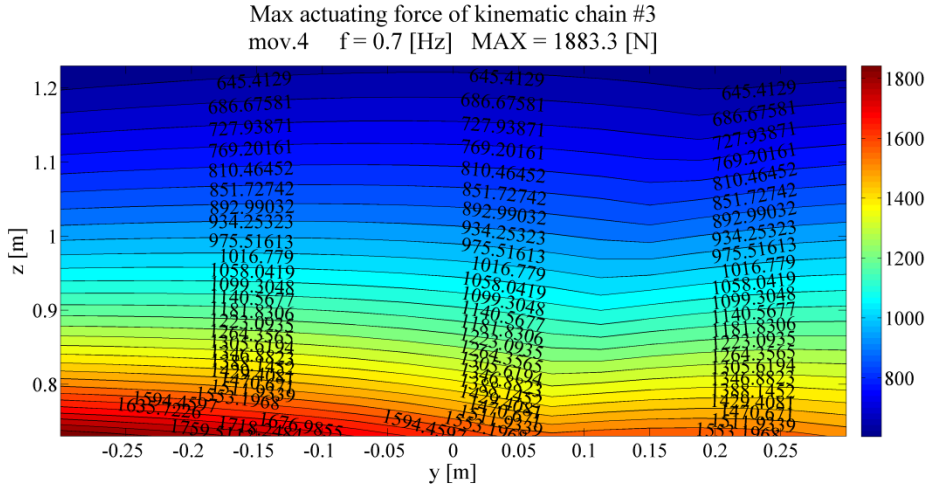

Figure 4-13 maximum actuating force of the kinematic chain 3, motion law: 4)mov.α

It can be seen that the most critical area of the operation of the robot in terms of the maximum actuating force is generally when the TCP of the platform is located in the bottom of workspace which is been expected.

Due to the symmetry of the architecture with respect to the xz reference plane the trend of the kinematic chains$6, 5,$ and 4 would be similar to the first three chains only mirrored respect to the z axis. It can be seen that the maximum value of actuating force among all the kinematic chains occur for the third and fourth, which are located more close to the xz plane of the reference frame.

As we discussed before in the dynamic analysis section, it is also possible to estimate the loads in the legs from the universal joints force in the extremities of the leg, by neglecting the inertia effects and considering the legs as two force element. In figure 4.14 the trend of the magnitude force of universal joint over the slider of the kinematic chain 1 is represented. We remind again that the magnitude force of the universal joints is slightly greater than the component of the force along the direction of the link, and by this choice we remain more in the safe area in terms of design of the links.

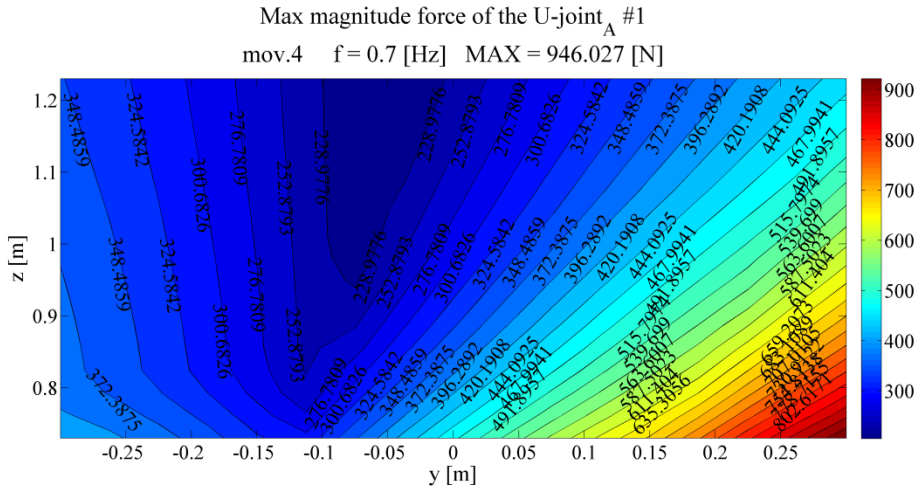

Figure 4-14 maximum U-joint magnitude force of the kinematic chain 1, motion law: 4)mov.α

It can be seen that the trend of the magnitude of the universal joint force is similar to the trend of the actuating force, only the values are increased due to the constraints reaction forces.

In figure 4.15 the position of the TCP inside the yz-plane of the workspace, corresponds to the maximum value of the actuating force of the first kinematic chain is represented. In this configuration, the TCP execute a sinusoidal rotation about the x axis of the reference frame, with the prescribed values of the y, z coordinates, and orientation about the y and z axis of the reference frame.

The position coordinate and orientation of the platform correspond to the operating condition of the TCP where maximum values of the forces of the joints occurs, are represented in appendix C. These data are given for all the kinematic chains and for the case of motion laws 2)mov.y, 3)mov.z, and 4)mov.α.

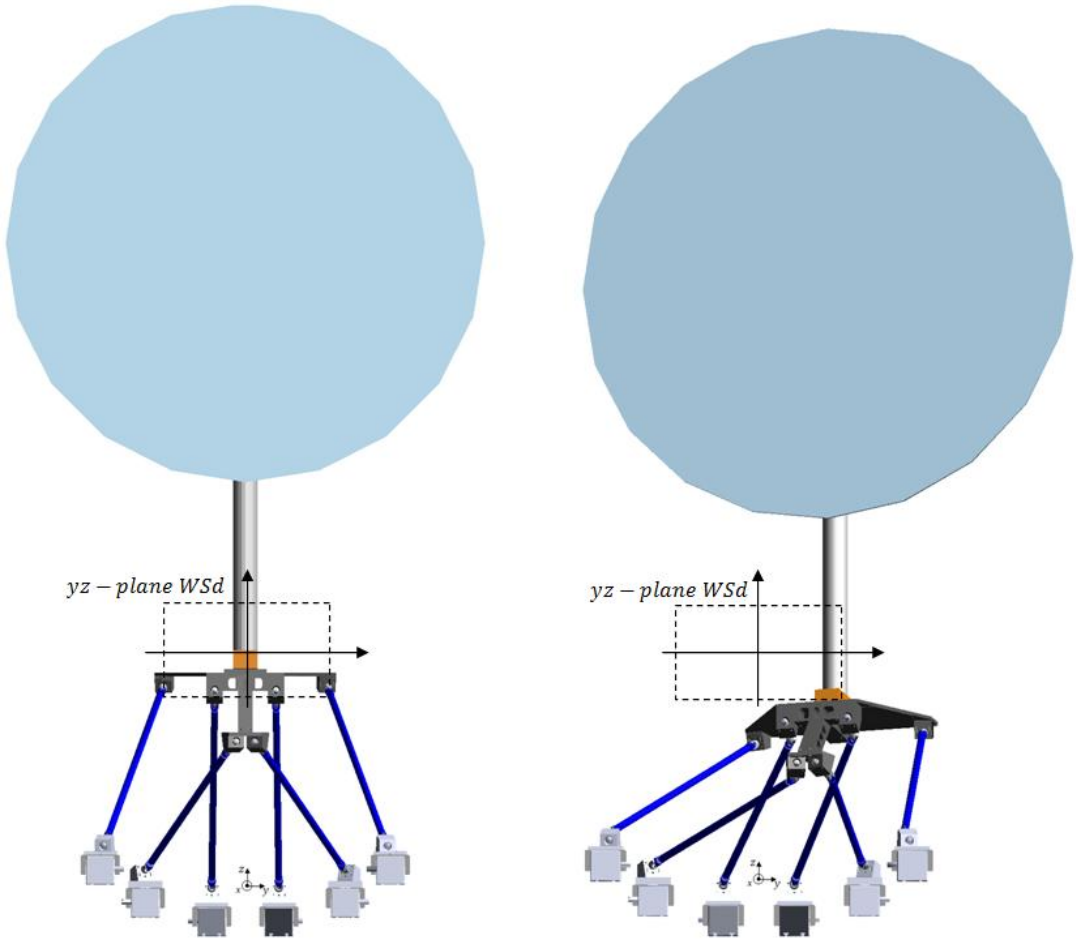

Figure 4-15 Left: Robot home position Right: Robot state correspond to maximum value of the linear actuating force of first kinematic chain

However when we deal with the component of the constraint reaction force of the sliding body along the z direction $F_{A_{i,z}}$ the situation is opposite. The value of the normal reaction force is increased when the platform operates at higher altitudes (Figures 4.18 – 4.19).

Again we would have a mirrored behavior between the first and last three kinematic chains due to the symmetry of the architecture described in chapter 2.

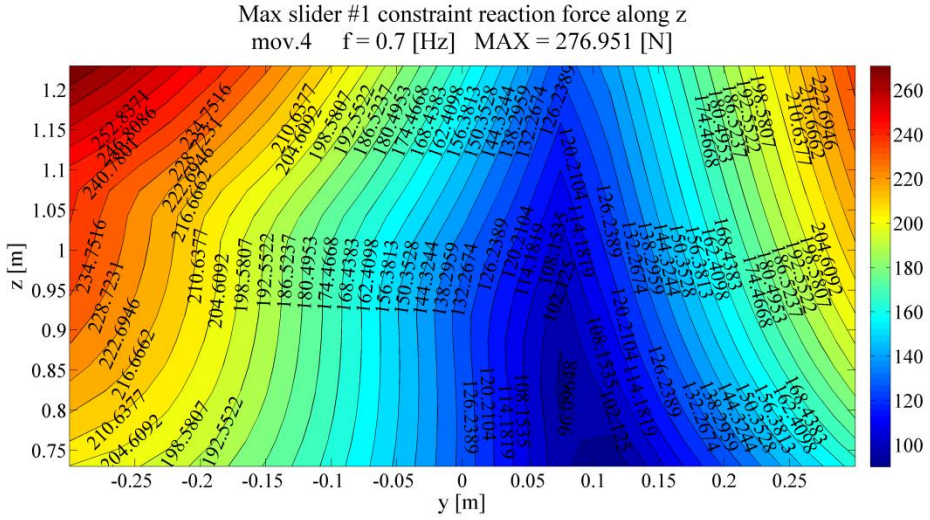

Figure 4-16 maximum slider reaction force $F_{A_{i,z}}$ for the first kinematic chain, motion law: 4)mov.α

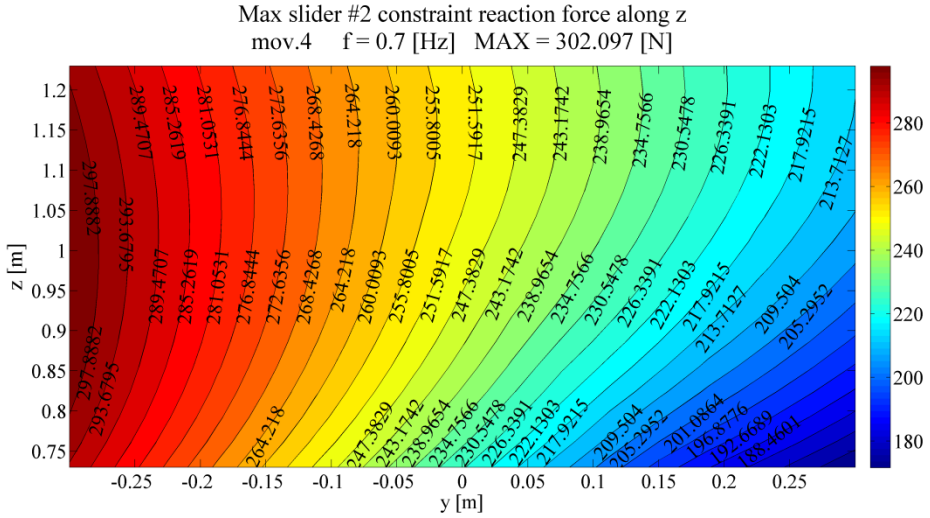

Figure 4-17 maximum slider reaction force $F_{A_{i,z}}$ for the second kinematic chain, motion law: 4)mov.α

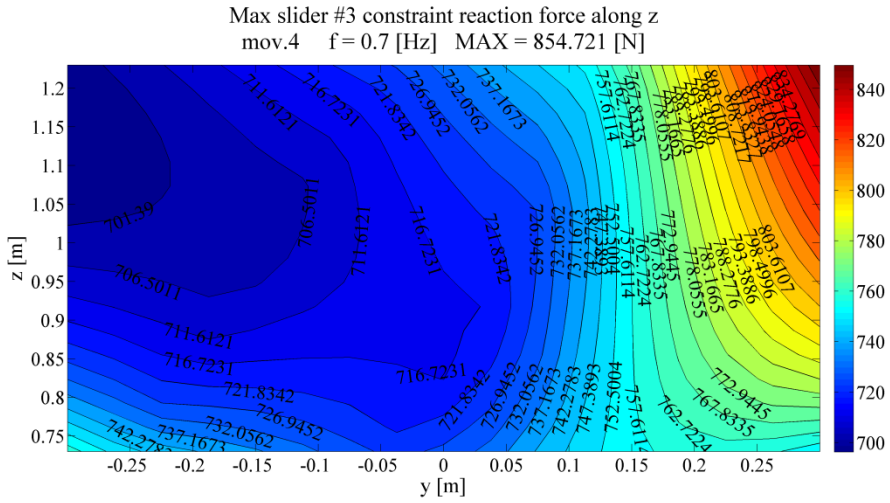

Figure 4-18 maximum slider reaction force $F_{A_{i,z}}$ for the second kinematic chain, motion law: 4)mov.α

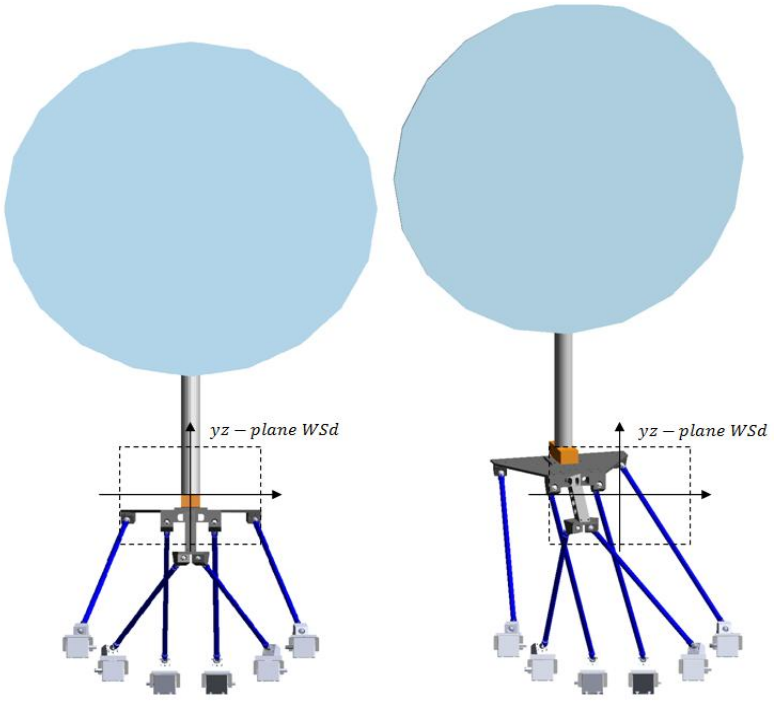

Figure 4-19 Left: Robot home position Right: Robot state correspond to maximum constraint reaction force $F_{A_{i,z}}$ of first kinematic chain

The symmetric dynamic behavior of the mechanism about the z axis of its desired workspace could be clearly evident by discussing the motion case 3 which is the sinusoidal movement of the TCP along the z axis. At each point of the grid along the y axis of the WSd a sinusoidal motion along the z axis has been imposed with all the possible combinations of the platform orientation. The results of the maximum value of the linear motion force and the constraint reaction along z axis of the sliders at correspond to each point of the y axis of the WSd is given in figure 4.20 – 4.21.

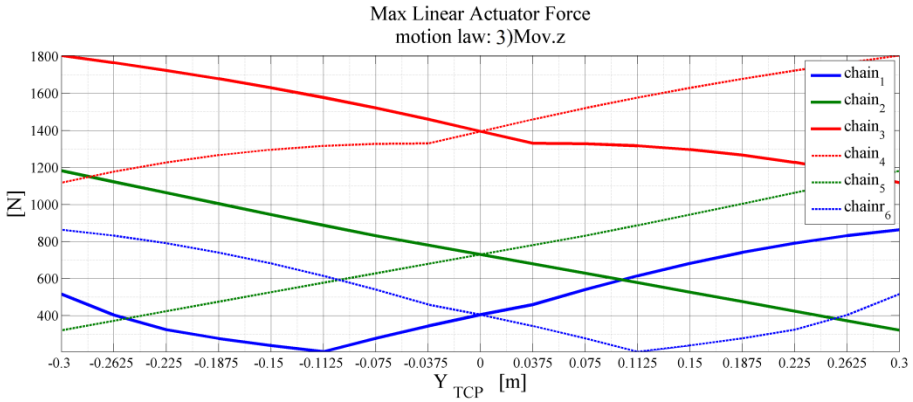

Figure 4-20 maximum actuating force of all the kinematic chains, motion law: 3)mov.z

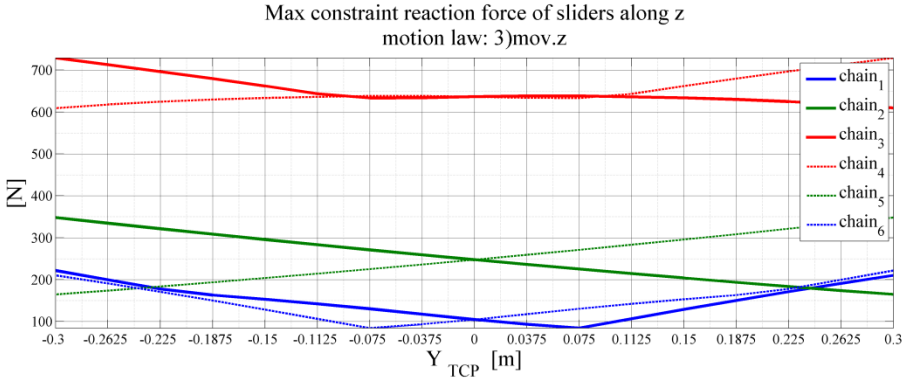

Figure 4-21 maximum slider constraint reaction force along z axis of all the kinematic chains, motion law: 3)mov.z

It can also be evident that when the TCP of the platform is operating at the boundaries of the WSd along the y direction, 3 kinematic chains are in the most

critical situation and the other 3 are in the safest condition, in terms of the dynamic loads.

In appendix C the maximum values of the dynamic loads of each kinematic chain for different operating condition of the platform described in table 4.1 are given separately.

In table 4.6 the maximum value of the actuating force and the constraint reaction forces and torques on the sliding body necessary for the choice of the linear actuator are given. These values are the evaluated maximum among all the described motion laws of table 4.1 simulations.

	Chain 1	Chain 2	Chain 3	Chain 4	Chain 5	Chain 6
$\max \lvert\tau_i(t)\rvert$ [N]	1397.45	1261.36	1980.60	2767.19	1737.65	1441.91
$\max\lvert F_{A_{i,y}}(t)\rvert$ [N]	741.17	260.44	467.12	533.40	239.75	672.50
$\max\lvert F_{A_{i,z}}(t)\rvert$ [N]	792.35	447.62	998.18	1079.75	548.58	831.20
$\max\lvert T_{A_{i,x}}(t)\rvert$ [N.m]	83.29	24.52	57.38	65.54	21.49	76.59
$\max\lvert T_{A_{i,y}}(t)\rvert$ [N.m]	145.40	113.58	205.76	287.98	156.92	143.93
$\max\lvert T_{A_{i,z}}(t)\rvert$ [N.m]	42.75	37.58	24.36	27.81	50.83	38.54

Table 4-6 maximum value of the loads on the sliders

Conclusion

The kinematics and dynamics of the 6-dof fully parallel mechanism based on PRRS kinematic chains have been studied. An analytical method to deal with the inverse kinematic problem of manipulators based on Hexaglide architecture and different family architecture with the capability of ensuring symmetric global workspace has been represented. Some drawbacks of the complexity of the dynamic model of parallel robots in practice have been discussed and a formalism based on Newton-Euler equation of motion for the solution of dynamic problem of the Hexaglide architecture is given.

With the aid of Adams multibody dynamics software a simulation model of the robot has been developed. To realize the dynamics of the robot for its operation condition, a method of dividing the workspace into grid of points has been applied. For the specific application of the platform to simulate the real working condition of the offshore wind turbine, different sets of motion laws at each point inside the working grid have been applied. The specifications of the motions have been chosen to have the most possible coincidence with the real working condition of the robot. The method of automating the work to deal with the huge number of simulations for the entire working grid by using macros has been given. The results of the dynamic simulation have been provided for decision making of design features.

It is possible to extend the application of the designed platform for other similar conditions such as sailboats maneuvers and other offshore structures. The future task is to develop the hardware in the loop simulation of the platform for the specific application.

Appendix A

A.1 Closed loop kinematic chain

These definitions are taken from C. Gosselin [8].

A *closed-loop kinematic chain* is obtained when one of the links, but not the base, possesses a connection degree greater than or equal to 3.

For each link of a manipulator, the *connection degree* is the number of rigid bodies attached to this link by a joint.

Simple kinematic chains are then defined as being those in which each member possesses a connection degree that is less than or equal to 2. Serial manipulators may then be defined as simple kinematic chains for which all the connection degrees are 2, except for two of them, the base and the end-effector, with connection degree 1. Such a chain is also called an *open-loop kinematic chain*.

A.2 Mobility

The general mobility criterion for spatial mechanisms is defined by Grubler's formula as:

$$m = 6(n - j - 1) + \sum_{i=1}^{j} f_i \tag{A.1}$$

Where n is the total number of rigid bodies, j is the number of joints, and f_i is the number of dof of each joint. Note that if m is negative the mechanism is assumed as *over constrained*. It is difficult, however, to define a general mobility criterion for closed loop kinematic chains. Classical mobility formulae can indeed lead us to ignore some degrees of freedom. Because, it does not take the geometric relations between the joints into consideration. For example, mechanism with 0 mobility, or even over constrained may have in fact finite mobility because of the dependency

between the constraints. Grubler's formula is nevertheless generally used.
Note that in the Grubler formula we just count the number of dof constrained by the joints. The technological means that will be used to realize these constraints do not play a role in the mobility of the mechanism. A direct consequence is that mechanisms that differ by their joint nature may be equivalent from a mobility view point. For example replacing a prismatic actuated joint by a revolute one (or by more complex components such as cams) in a given mechanism will not change the mobility (but may have an high impact on other kinematic performances) [7].

Appendix B

B.1 Euler angles

The most classical way to define the orientation of a rigid body in space is introduced by Euler angles. Different authors may use different sets of rotation axes to define Euler angles, or different names for the same angles.

In the *proper Euler angles* set the first and the last rotation axis are same. Therefore, there are six possibilities of choosing the rotation axes for proper Euler angles:

$$\begin{cases} z - x' - z'' \\ x - y' - x'' \\ y - z' - y'' \\ z - y' - z'' \\ x - z' - x'' \\ y - x' - y'' \end{cases} \tag{B.1}$$

For example in the first set, *z-x'-z″* the angles are defined as:

α: Rotation along the z axis of the frame

β: Rotation angle along the x axis of the new frame

γ: Rotation angle along the z axis of the new frame

Another common method is the Tait-Bryan angles also known as yaw, pitch and roll or nautical angles. The definitions and notations used for Tait-Bryan angles are similar to those described above for proper Euler angles. The only difference is that Tait–Bryan angles represent rotations about three distinct axes.

There are six possibilities of choosing the rotation axes for Tait–Bryan angles. The six possible sequences are:

$$\begin{cases} x - y' - z'' \\ y - z' - x'' \\ z - x' - y'' \\ x - z' - y'' \\ z - y' - x'' \\ y - x' - z'' \end{cases} \quad \text{(B.2)}$$

For instance in the third set, *z-x'-y″* the angles are defined as:

α: Rotation along the z axis of the frame

β: Rotation angle along the x axis of the new frame

γ: Rotation angle along the y axis of the new frame

B.2 Rotation matrix:

The rotation matrix between the fixed and oriented frame depends on the choice of the set of Euler angles.

For example in case of the proper Euler angles, *z-x'-z″* we have:

$$R_{01} = \begin{bmatrix} c(\alpha) & -s(\alpha) & 0 \\ s(\alpha) & c(\alpha) & 0 \\ 0 & 0 & 1 \end{bmatrix} \quad \text{(B.3)}$$

$$R_{12} = \begin{bmatrix} 1 & 0 & 0 \\ 0 & c(\beta) & -s(\beta) \\ 0 & s(\beta) & c(\beta) \end{bmatrix} \quad \text{(B.4)}$$

$$R_{23} = \begin{bmatrix} c(\gamma) & -s(\gamma) & 0 \\ s(\gamma) & c(\gamma) & 0 \\ 0 & 0 & 1 \end{bmatrix} \quad \text{(B.5)}$$

$$R_{03} = R_{01}R_{12}R_{23}$$
$$= \begin{bmatrix} c(\alpha)c(\gamma) - s(\alpha)c(\beta)s(\gamma) & -c(\alpha)s(\gamma) - c(\beta)c(\gamma)s(\alpha) & s(\alpha)s(\beta) \\ s(\alpha)c(\gamma) + c(\alpha)c(\beta)s(\gamma) & c(\alpha)c(\beta)c(\gamma) - s(\alpha)s(\gamma) & -c(\alpha)s(\beta) \\ s(\beta)s(\gamma) & c(\gamma)s(\beta) & c(\beta) \end{bmatrix} \quad \text{(B.6)}$$

For the Tait-Bryan angles , *z-y'-x″ :*

$$R_{01} = \begin{bmatrix} c(\alpha) & -s(\alpha) & 0 \\ s(\alpha) & c(\alpha) & 0 \\ 0 & 0 & 1 \end{bmatrix} \quad \text{(B.7)}$$

$$R_{12} = \begin{bmatrix} c(\beta) & 0 & s(\beta) \\ 0 & 1 & 0 \\ -s(\beta) & 0 & c(\beta) \end{bmatrix} \quad \text{(B.8)}$$

$$R_{12} = \begin{bmatrix} 1 & 0 & 0 \\ 0 & c(\gamma) & -s(\gamma) \\ 0 & s(\gamma) & c(\gamma) \end{bmatrix} \quad \text{(B.9)}$$

$$R_{03} = R_{01}R_{12}R_{23}$$
$$= \begin{bmatrix} c(\alpha)c(\gamma) - s(\alpha)s(\beta)s(\gamma) & -c(\beta)s(\alpha) & c(\alpha)s(\gamma) + c(\gamma)s(\alpha)s(\beta) \\ s(\alpha)c(\gamma) + c(\alpha)s(\beta)s(\gamma) & c(\alpha)c(\beta) & s(\alpha)s(\gamma) - c(\alpha)c(\gamma)s(\beta) \\ -c(\beta)s(\gamma) & s(\beta) & c(\beta)c(\gamma) \end{bmatrix} \quad \text{(B.10)}$$

B.3 Skew symmetric angular velocity matrix:

We can define the point P projected in frame $O - xyz$ as:

$$P = C + Rb' \quad \text{(B.11)}$$

Where b' is the vector of position of point B in the rotating frame $C - x'y'z'$, and R is the orthogonal rotation matrix between the two frame:

$$b = Rb' \tag{B.12}$$

Taking the derivative of this equation and assume that the vector b' is constant we will have:

$$v_P = v_C + \frac{dR}{dt}b' = v_C + \frac{dR}{dt}R^T b \tag{B.13}$$

We define the angular velocity matrix as:

$$\Omega = \frac{dR}{dt}R^T \tag{B.14}$$

Since the rotation matrix is an orthogonal matrix we can demonstrate that the angular velocity matrix is a skew symmetric type:

$$\Omega = -\Omega^T = \begin{bmatrix} 0 & -\omega_z & \omega_y \\ \omega_z & 0 & -\omega_x \\ -\omega_y & \omega_x & 0 \end{bmatrix} \tag{B.15}$$

The expression of the components of the angular velocity matrix depends on the choice of the sequence of the rotation angles. For instance, in case of the Tait-Bryan angles , *z-y'-x″* we would have:

$$\begin{aligned} \Omega &= \frac{dR}{dt}R^T \\ &= \begin{bmatrix} 0 & -\dot{\beta}s(\alpha) - \dot{\gamma}c(\alpha)c(\beta) & \dot{\beta}c(\alpha) - \gamma c(\beta)\dot{)}s(\alpha) \\ \dot{\beta}s(\alpha) + \dot{\gamma}c(\alpha)c(\beta) & 0 & -\dot{\alpha} - \dot{\gamma}s(\beta) \\ -\dot{\beta}c(\alpha) + \gamma c(\beta)\dot{)}s(\alpha) & \dot{\alpha} + \dot{\gamma}s(\beta) & 0 \end{bmatrix} \end{aligned} \tag{B.16}$$

The relation between the vector and matrix of angular velocity can be defined as:

$$\Omega b = \omega \times b \tag{B.14}$$

Appendix C

In this section some tables of results of the simulation of the dynamic model of the mechanism are represented. In these tables, for all the kinematic chains the maximum value of the dynamic loads, together with the corresponding configuration of the platform position and orientation are represented.

The position coordinate of the platform projected in the fixed reference frame is represented by $[x_{TCP} \quad y_{TCP} \quad z_{TCP}]$, and the orientation of the platform is defined by $[\alpha \quad \beta \quad \gamma]$, which are the rotation angle of the platform about the x, y, and z axis of the reference frame respectively.

The forces and torques are introduced with the same notation defined in the design chapter and the magnitude value of the forces of the universal joints at the base and platform connection are defined as UA_i and UB_i respectively, for each kinematic chain.

	$\alpha = 15\sin(2\pi f t)$ $[deg]$ $, f = 0.7[Hz]$				
	max value	z_{TCP} [mm]	y_{TCP} [mm]	β [deg]	γ [deg]
$\lvert\tau_1(t)\rvert$ [N]	783.03	-250	300	-15	-15
$\lvert\tau_2(t)\rvert$ [N]	1068.38	-250	-300	0	-15
$\lvert\tau_3(t)\rvert$ [N]	1883.30	-250	-300	15	15
$\lvert\tau_4(t)\rvert$ [N]	1883.03	-250	300	15	-15
$\lvert\tau_5(t)\rvert$ [N]	1068.24	-250	300	0	15
$\lvert\tau_6(t)\rvert$ [N]	782.85	-250	-300	-15	15
$\lvert UA_1(t)\rvert$ [N]	946.03	-250	300	-15	-15
$\lvert UA_2(t)\rvert$ [N]	1086.18	-250	-300	0	-15
$\lvert UA_3(t)\rvert$ [N]	2017.48	-250	-300	15	15
$\lvert UA_4(t)\rvert$ [N]	2017.20	-250	300	15	-15
$\lvert UA_5(t)\rvert$ [N]	1086.05	-250	300	0	15
$\lvert UA_6(t)\rvert$ [N]	945.77	-250	-300	-15	15
$\lvert UB_1(t)\rvert$ [N]	949.44	-250	300	-15	-15
$\lvert UB_2(t)\rvert$ [N]	1080.89	-250	-300	0	-15
$\lvert UB_3(t)\rvert$ [N]	2009.48	-250	-300	15	15

$\lvert UB_4(t)\rvert$ [N]	2009.20	-250	300	15	-15
$\lvert UB_5(t)\rvert$ [N]	1080.76	-250	300	0	15
$\lvert UB_6(t)\rvert$ [N]	949.18	-250	-300	-15	15
$\lvert F_{A_{1,z}}(t)\rvert$ [N]	276.95	250	-300	15	15
$\lvert F_{A_{2,z}}(t)\rvert$ [N]	302.10	0	-300	15	-15
$\lvert F_{A_{3,z}}(t)\rvert$ [N]	854.72	250	300	-15	-15
$\lvert F_{A_{4,z}}(t)\rvert$ [N]	854.48	250	-300	-15	15
$\lvert F_{A_{5,z}}(t)\rvert$ [N]	302.06	0	300	15	15
$\lvert F_{A_{6,z}}(t)\rvert$ [N]	276.96	250	300	15	-15
$\lvert F_{A_{1,y}}(t)\rvert$ [N]	584.20	-250	300	0	15
$\lvert F_{A_{2,y}}(t)\rvert$ [N]	197.77	-250	263	-15	-15
$\lvert F_{A_{3,y}}(t)\rvert$ [N]	467.12	-250	300	-15	15
$\lvert F_{A_{4,y}}(t)\rvert$ [N]	466.95	-250	-300	-15	-15
$\lvert F_{A_{5,y}}(t)\rvert$ [N]	197.73	-250	-262	-15	15
$\lvert F_{A_{6,y}}(t)\rvert$ [N]	584.03	-250	-300	0	-15
$\lvert \mathrm{T}_{\mathrm{A}_{1,x}}(\mathrm{t})\rvert$ [N.m]	67.42	-250	300	0	15
$\lvert \mathrm{T}_{\mathrm{A}_{2,x}}(\mathrm{t})\rvert$ [N.m]	17.55	-250	300	-15	-15
$\lvert \mathrm{T}_{\mathrm{A}_{3,x}}(\mathrm{t})\rvert$ [N.m]	57.38	-250	300	-15	15
$\lvert \mathrm{T}_{\mathrm{A}_{4,x}}(\mathrm{t})\rvert$ [N.m]	57.36	-250	-300	-15	-15
$\lvert \mathrm{T}_{\mathrm{A}_{5,x}}(\mathrm{t})\rvert$ [N.m]	17.54	-250	-300	-15	15
$\lvert \mathrm{T}_{\mathrm{A}_{6,x}}(\mathrm{t})\rvert$ [N.m]	67.40	-250	-300	0	-15
$\lvert \mathrm{T}_{\mathrm{A}_{1,y}}(\mathrm{t})\rvert$ [N.m]	77.49	-250	300	-15	-15
$\lvert \mathrm{T}_{\mathrm{A}_{2,y}}(\mathrm{t})\rvert$ [N.m]	95.78	-250	-300	0	-15
$\lvert \mathrm{T}_{\mathrm{A}_{3,y}}(\mathrm{t})\rvert$ [N.m]	195.02	-250	-300	15	15
$\lvert \mathrm{T}_{\mathrm{A}_{4,y}}(\mathrm{t})\rvert$ [N.m]	194.99	-250	300	15	-15
$\lvert \mathrm{T}_{\mathrm{A}_{5,y}}(\mathrm{t})\rvert$ [N.m]	95.76	-250	300	0	15
$\lvert \mathrm{T}_{\mathrm{A}_{6,y}}(\mathrm{t})\rvert$ [N.m]	77.48	-221	-265	-15	15
$\lvert \mathrm{T}_{\mathrm{A}_{1,z}}(\mathrm{t})\rvert$ [N.m]	33.64	-250	300	0	15
$\lvert \mathrm{T}_{\mathrm{A}_{2,z}}(\mathrm{t})\rvert$ [N.m]	31.96	-250	-300	0	-15
$\lvert \mathrm{T}_{\mathrm{A}_{3,z}}(\mathrm{t})\rvert$ [N.m]	24.36	-250	300	-15	15
$\lvert \mathrm{T}_{\mathrm{A}_{4,z}}(\mathrm{t})\rvert$ [N.m]	24.35	-250	-300	-15	-15

$\lvert T_{A_{5,z}}(t)\rvert$ [N.m]	31.96	-250	300	0	15
$\lvert T_{A_{6,z}}(t)\rvert$ [N.m]	33.62	-250	-300	0	-15

Table C.1 maximum value of dynamic loads for the motion law: 4)mov.α

		$y = 0.3\sin(2\pi f t)$ $[m]$, $f = 0.7[Hz]$			
	max value	z_{TCP} [mm]	α [deg]	β [deg]	γ [deg]
$\lvert\tau_1(t)\rvert$ [N]	1397.45	-250	-15	15	-15
$\lvert\tau_2(t)\rvert$ [N]	1261.36	-250	15	0	-15
$\lvert\tau_3(t)\rvert$ [N]	1980.60	-250	15	15	15
$\lvert\tau_4(t)\rvert$ [N]	2767.19	-250	-15	15	-15
$\lvert\tau_5(t)\rvert$ [N]	1737.65	-250	-15	0	15
$\lvert\tau_6(t)\rvert$ [N]	1441.91	-250	-15	-15	15
$\lvert UA_1(t)\rvert$ [N]	1480.70	-250	-15	15	-15
$\lvert UA_2(t)\rvert$ [N]	1284.07	-250	15	0	-15
$\lvert UA_3(t)\rvert$ [N]	2129.04	-250	15	15	15
$\lvert UA_4(t)\rvert$ [N]	2969.45	-250	-15	15	-15
$\lvert UA_5(t)\rvert$ [N]	1766.11	-250	-15	0	15
$\lvert UA_6(t)\rvert$ [N]	1485.85	-250	-15	-15	15
$\lvert UB_1(t)\rvert$ [N]	1476.49	-250	-15	15	-15
$\lvert UB_2(t)\rvert$ [N]	1279.42	-250	15	0	-15
$\lvert UB_3(t)\rvert$ [N]	2123.06	-250	15	15	15
$\lvert UB_4(t)\rvert$ [N]	2964.53	-250	-15	15	-15
$\lvert UB_5(t)\rvert$ [N]	1761.05	-250	-15	0	15
$\lvert UB_6(t)\rvert$ [N]	1479.33	-250	-15	-15	15
$\lvert F_{A_{1,z}}(t)\rvert$ [N]	792.35	250	0	-15	-15
$\lvert F_{A_{2,z}}(t)\rvert$ [N]	430.35	250	-15	-15	-15
$\lvert F_{A_{3,z}}(t)\rvert$ [N]	798.11	-250	15	15	15
$\lvert F_{A_{4,z}}(t)\rvert$ [N]	1079.75	-250	-15	15	-15
$\lvert F_{A_{5,z}}(t)\rvert$ [N]	548.58	250	15	-15	15
$\lvert F_{A_{6,z}}(t)\rvert$ [N]	831.20	250	-15	-15	15
$\lvert F_{A_{1,y}}(t)\rvert$ [N]	741.17	-125	15	-15	15
$\lvert F_{A_{2,y}}(t)\rvert$ [N]	260.44	-250	15	-15	-15

$\lvert F_{A_{3,y}}(t)\rvert$ [N]	440.80	-250	15	15	15
$\lvert F_{A_{4,y}}(t)\rvert$ [N]	533.40	-250	15	15	0
$\lvert F_{A_{5,y}}(t)\rvert$ [N]	108.37	-250	-15	15	-15
$\lvert F_{A_{6,y}}(t)\rvert$ [N]	611.53	-250	-15	-15	-15
$\lvert T_{A_{1,x}}(t)\rvert$ [N.m]	83.29	-187	15	-15	15
$\lvert T_{A_{2,x}}(t)\rvert$ [N.m]	24.52	-250	15	-15	-15
$\lvert T_{A_{3,x}}(t)\rvert$ [N.m]	54.16	-250	15	15	15
$\lvert T_{A_{4,x}}(t)\rvert$ [N.m]	65.54	-250	15	15	0
$\lvert T_{A_{5,x}}(t)\rvert$ [N.m]	16.80	250	15	-15	15
$\lvert T_{A_{6,x}}(t)\rvert$ [N.m]	69.64	-250	-15	-15	-15
$\lvert T_{A_{1,y}}(t)\rvert$ [N.m]	145.40	-250	-15	15	-15
$\lvert T_{A_{2,y}}(t)\rvert$ [N.m]	113.58	-250	15	0	-15
$\lvert T_{A_{3,y}}(t)\rvert$ [N.m]	205.76	-250	15	15	15
$\lvert T_{A_{4,y}}(t)\rvert$ [N.m]	287.98	-250	-15	15	-15
$\lvert T_{A_{5,y}}(t)\rvert$ [N.m]	156.92	-250	-15	0	15
$\lvert T_{A_{6,y}}(t)\rvert$ [N.m]	143.93	-250	-15	-15	15
$\lvert T_{A_{1,z}}(t)\rvert$ [N.m]	42.75	-125	15	-15	15
$\lvert T_{A_{2,z}}(t)\rvert$ [N.m]	37.58	-250	15	0	-15
$\lvert T_{A_{3,z}}(t)\rvert$ [N.m]	22.98	-250	15	15	15
$\lvert T_{A_{4,z}}(t)\rvert$ [N.m]	27.81	-250	15	15	0
$\lvert T_{A_{5,z}}(t)\rvert$ [N.m]	50.83	-250	-15	0	15
$\lvert T_{A_{6,z}}(t)\rvert$ [N.m]	35.08	-250	-15	-15	-15

Table C.2 maximum value of dynamic loads for the motion law: 2)mov.y

		$z = 0.25\sin(2\pi ft)$ $[m]$ $, f = 0.7[Hz]$			
	max value	y_{TCP} [mm]	α [deg]	β [deg]	γ [deg]
$\lvert \tau_1(t)\rvert$ [N]	863.61	300	15	-15	-15
$\lvert \tau_2(t)\rvert$ [N]	1182.64	-300	15	0	-15
$\lvert \tau_3(t)\rvert$ [N]	1804.93	-300	15	15	15
$\lvert \tau_4(t)\rvert$ [N]	1804.41	300	-15	15	-15
$\lvert \tau_5(t)\rvert$ [N]	1182.47	300	-15	0	15

$\lvert\tau_6(t)\rvert$ [N]	863.44	-300	-15	-15	15
$\lvert UA_1(t)\rvert$ [N]	1068.84	300	15	-15	-15
$\lvert UA_2(t)\rvert$ [N]	1197.74	-300	15	0	-15
$\lvert UA_3(t)\rvert$ [N]	1921.32	-300	15	15	15
$\lvert UA_4(t)\rvert$ [N]	1920.76	300	-15	15	-15
$\lvert UA_5(t)\rvert$ [N]	1197.57	300	-15	0	15
$\lvert UA_6(t)\rvert$ [N]	1068.63	-300	-15	-15	15
$\lvert UB_1(t)\rvert$ [N]	1076.66	300	15	-15	-15
$\lvert UB_2(t)\rvert$ [N]	1190.84	-300	15	0	-15
$\lvert UB_3(t)\rvert$ [N]	1909.99	-300	15	15	15
$\lvert UB_4(t)\rvert$ [N]	1909.43	300	-15	15	-15
$\lvert UB_5(t)\rvert$ [N]	1190.67	300	-15	0	15
$\lvert UB_6(t)\rvert$ [N]	1076.45	-300	-15	-15	15
$\lvert F_{A_{1,z}}(t)\rvert$ [N]	221.52	-300	0	-15	-15
$\lvert F_{A_{2,z}}(t)\rvert$ [N]	348.22	-300	-15	15	-15
$\lvert F_{A_{3,z}}(t)\rvert$ [N]	729.21	-300	15	15	15
$\lvert F_{A_{4,z}}(t)\rvert$ [N]	729.02	300	-15	15	-15
$\lvert F_{A_{5,z}}(t)\rvert$ [N]	348.19	300	15	15	15
$\lvert F_{A_{6,z}}(t)\rvert$ [N]	221.55	300	0	-15	15
$\lvert F_{A_{1,y}}(t)\rvert$ [N]	672.59	300	15	-15	15
$\lvert F_{A_{2,y}}(t)\rvert$ [N]	157.68	113	15	-15	-15
$\lvert F_{A_{3,y}}(t)\rvert$ [N]	382.75	300	15	-15	15
$\lvert F_{A_{4,y}}(t)\rvert$ [N]	382.56	-300	-15	-15	-15
$\lvert F_{A_{5,y}}(t)\rvert$ [N]	157.63	-112	-15	-15	15
$\lvert F_{A_{6,y}}(t)\rvert$ [N]	672.50	-300	-15	-15	-15
$\lvert \mathrm{T}_{\mathrm{A}_{1,x}}(\mathrm{t})\rvert$ [N.m]	76.60	300	15	-15	15
$\lvert \mathrm{T}_{\mathrm{A}_{2,x}}(\mathrm{t})\rvert$ [N.m]	13.22	-300	-15	15	0
$\lvert \mathrm{T}_{\mathrm{A}_{3,x}}(\mathrm{t})\rvert$ [N.m]	47.02	300	15	-15	15
$\lvert \mathrm{T}_{\mathrm{A}_{4,x}}(\mathrm{t})\rvert$ [N.m]	46.99	-300	-15	-15	-15
$\lvert \mathrm{T}_{\mathrm{A}_{5,x}}(\mathrm{t})\rvert$ [N.m]	13.21	300	15	15	0
$\lvert \mathrm{T}_{\mathrm{A}_{6,x}}(\mathrm{t})\rvert$ [N.m]	76.59	-300	-15	-15	-15
$\lvert \mathrm{T}_{\mathrm{A}_{1,y}}(\mathrm{t})\rvert$ [N.m]	86.96	300	15	-15	-15

$\lvert T_{A_{2,y}}(t)\rvert$ [N.m]	105.77	-300	15	0	-15
$\lvert T_{A_{3,y}}(t)\rvert$ [N.m]	185.77	-300	15	15	15
$\lvert T_{A_{4,y}}(t)\rvert$ [N.m]	185.72	300	-15	15	-15
$\lvert T_{A_{5,y}}(t)\rvert$ [N.m]	105.75	300	-15	0	15
$\lvert T_{A_{6,y}}(t)\rvert$ [N.m]	86.94				
$\lvert T_{A_{1,z}}(t)\rvert$ [N.m]	38.54	300	15	-15	15
$\lvert T_{A_{2,z}}(t)\rvert$ [N.m]	35.21	-300	15	0	-15
$\lvert T_{A_{3,z}}(t)\rvert$ [N.m]	19.95	300	15	-15	15
$\lvert T_{A_{4,z}}(t)\rvert$ [N.m]	19.95	-300	-15	-15	-15
$\lvert T_{A_{5,z}}(t)\rvert$ [N.m]	35.21	300	-15	0	15
$\lvert T_{A_{6,z}}(t)\rvert$ [N.m]	38.54	-300	-15	-15	-15

Table C.3 maximum value of dynamic loads for the motion law: 3)mov.z

References

[1] Owinnett, James E. "Amusement device." U.S. Patent 1,789,680, issued January 20, 1931.

[2] Bonev I.A. The true origins of parallel robots. January, 24, 2003,

[3] Stewart, Doug. "A platform with six degrees of freedom." Proceedings of the institution of mechanical engineers 180, no. 1 (1965): 371-386.

[4] "Machines for the 21st Century", Machinery and Production Engineering, Vol. 153,No. 3886, pp. 20-25, 1995.

[5] Grace, Kenneth Wayne. "Kinematic design of an ophthalmic surgery robot and feature extracting bilateral manipulation." PhD diss., Northwestern University, 1995.

[6] Lazarevic, Zoran. "Feasibility of a Stewart Platform with fixed actuators as a platform for CABG surgery device." *Master's Thesis (Oct. 10, 1997)* (1997).

[7] Merlet, Jean-Pierre. "Parallel robots, volume 128 of solid mechanics and its applications." (2006).

[8] Gosselin C. *Kinematic analysis optimization and programming of parallel robotic manipulators*. Ph.D. Thesis, McGill University, Montr´eal,June, 15, 1988.

[9] Tanev, Tanio K. "Kinematics of a hybrid (parallel–serial) robot manipulator." *Mechanism and Machine Theory* 35, no. 9 (2000): 1183-1196.

[10] Bonev, Ilian Alexandrov. "Analysis and design of 6-DOF 6-PRRS parallel manipulators." *Master Thesis, Kwangju Institute of Science and Technology, Kwangju* (1998).

[11] Ferrari, Davide. "Hexafloat: progettazione di una piattaforma robotica a 6-GDL con architettura a cinematica parallela di tipo Hexaglide." (2013).

[12] Toyoda, “Parallel Mechanism Based Milling Machine”, Cat. No. 96 1110-0 JO, 1996.

[13] Pritschow, G., C. Eppler, and W. D. Lehner. "Highly dynamic drives for parallel kinematic machines with constant arm length." In *1st Int. Colloquium, Collaborative Research Centre*, vol. 562, pp. 199-211. 2002.

[14] Honegger, Marcel, Alain Codourey, and Etienne Burdet. "Adaptive control of the Hexaglide, a 6 dof parallel manipulator." In *Robotics and Automation, 1997. Proceedings., 1997 IEEE International Conference on*, vol. 1, pp. 543-548. IEEE, 1997.

[15] Hunt, K. H. "Structural kinematics of in-parallel-actuated robot-arms." ASME, 1983.

[16] Pierrot, François. "Robots pleinementparallèleslégers: conception, modélisation et commande." PhD diss., 1991.

[17] Uchiyama, Masaru. "A 6 dof parallel robot HEXA." *Advanced Robotics* 8, no. 6 (1993): 601-601.

[18] Shelef, Gad. "Six degrees of freedom micromanipulator." U.S. Patent 4,819,496, issued April 11, 1989.

[19] Blajer, Wojciech, Werner Schiehlen, and Walter Schirm. "Dynamic analysis of constrained multibody systems using inverse kinematics." *Mechanism and machine theory* 28, no. 3 (1993): 397-405.

[20] Codourey, Alain, and Etienne Burdet. "A body-oriented method for finding a linear form of the dynamic equation of fully parallel robots." In *Robotics and Automation, 1997. Proceedings., 1997 IEEE International Conference on*, vol. 2, pp. 1612-1618. IEEE, 1997.

[21] Dasgupta, Bhaskar, and Prasun Choudhury. "A general strategy based on the Newton–Euler approach for the dynamic formulation of parallel manipulators."*Mechanism and Machine Theory* 34, no. 6 (1999): 801-824.

[22] Geng, Zheng, Leonard S. Haynes, James D. Lee, and Robert L. Carroll. "On the dynamic model and kinematic analysis of a class of Stewart platforms."*Robotics and Autonomous Systems* 9, no. 4 (1992): 237-254.

[23] Miller, K., and ReymondClavel. "The Lagrange-based model of Delta-4 robot dynamics." *Robotersysteme* 8, no. 1 (1992): 49-54.

[24] Zanganeh, Kourosh E., Rosario Sinatra, and Jorge Angeles. "Kinematics and dynamics of a six-degree-of-freedom parallel manipulator with revolute legs."*Robotica* 15, no. 04 (1997): 385-394

[25] Honegger, Marcel, Alain Codourey, and Etienne Burdet. "Adaptive control of the Hexaglide, a 6 dof parallel manipulator." In *Robotics and Automation, 1997. Proceedings., 1997 IEEE International Conference on*, vol. 1, pp. 543-548. IEEE, 1997.

[26] Gough, V. E. "Contribution to discussion of papers on research in automobile stability, control and tyre performance." In *Proc. Auto Div. Inst. Mech. Eng*, vol. 171, pp. 392-394. 1956.

[27] McCallion, H., and P. D. Truong. "The analysis of a six degree of freedom work station for mechanized assembly." In *Proc. 5th World Congress on Theory of Machines and Mechanisms*, vol. 611, p. 616. 1979.